A TRIDENT SCHOLAR PROJECT REPORT

NO. 451

Measurement and Modeling of High Energy Laser (HEL)-Droplet Interactions

by

Midshipman 1/C Timothy E. Tracey, USN

UNITED STATES NAVAL ACADEMY
ANNAPOLIS, MARYLAND

Measurement and Modeling of High Energy Laser (HEL)-Droplet Interactions

by

Midshipman 1/C Timothy E. Tracey
United States Naval Academy
Annapolis, Maryland

_____

Certification of Advisors' Approval

Associate Professor Cody Brownell
Mechanical Engineering Department

_____

_____

CDR Stuart Blair, USN
Mechanical Engineering Department

_____

_____

Acceptance for the Trident Scholar Committee

Professor Maria J. Schroeder
Associate Director of Midshipman Research

_____

_____

REPORT DOCUMENTATION PAGE

Form Approved
OMB No. 0704-0188

1. REPORT DATE *(DD-MM-YYYY)* 05-11-2016	**2. REPORT TYPE**	**3. DATES COVERED** *(From - To)*

4. TITLE AND SUBTITLE
Measurement and Modeling of High Energy Laser (HEL)-Droplet Interactions

5a. CONTRACT NUMBER

5b. GRANT NUMBER

5c. PROGRAM ELEMENT NUMBER

6. AUTHOR(S)
Tracey, Timothy E.

5d. PROJECT NUMBER

5e. TASK NUMBER

5f. WORK UNIT NUMBER

7. PERFORMING ORGANIZATION NAME(S) AND ADDRESS(ES)

8. PERFORMING ORGANIZATION REPORT NUMBER

9. SPONSORING / MONITORING AGENCY NAME(S) AND ADDRESS(ES)
U.S. Naval Academy
Annapolis, MD 21402

10. SPONSOR/MONITOR'S ACRONYM(S)

11. SPONSOR/MONITOR'S REPORT NUMBER(S)
Trident Scholar Report no. 451 (2016)

12. DISTRIBUTION / AVAILABILITY STATEMENT

This document has been approved for public release; its distribution is UNLIMITED.

13. SUPPLEMENTARY NOTES

14. ABSTRACT

   With the advent of lasers as weapons, it is necessary to understand how a laser propagates through a complex medium. For the U.S. Navy, the complexity of a maritime environment imposes particular challenges for laser propagation due to high concentrations of water vapor and high probabilities of liquid water in the form of fog, rain, or sea spray along the beam path. Although considerable research has gone into characterizing the maritime environment and simulating laser propagation through water vapor and turbulence, the interactions between a high energy laser (HEL) and liquid water are poorly understood.

   A project is taking place in the U.S. Naval Academy's Directed Energy Research Center to investigate the interaction of a high energy laser and single water droplets. An HEL is used to irradiate droplets of water, and the droplet shape and size, the infrared radiation from the droplet, and the transmitted beam profile are measured and recorded. To control the droplet shape, it will be levitated using a commercial ultrasonic levitator, where the drop is held in place at a node by the pressure from a standing sound wave. The results of this experiment will provide an understanding of the coupled interaction between an HEL and a water droplet.

15. SUBJECT TERMS
High Energy Laser (HEL), Droplet, Vaporization Regime, Directed Energy, LaWS

16. SECURITY CLASSIFICATION OF:			**17. LIMITATION OF ABSTRACT**	**18. NUMBER OF PAGES**	**19a. NAME OF RESPONSIBLE PERSON**
a. REPORT	**b. ABSTRACT**	**c. THIS PAGE**		74	**19b. TELEPHONE NUMBER** *(include area code)*

Standard Form 298 (Rev. 8-98)
Prescribed by ANSI Std. Z39.18

Abstract:

With the advent of lasers as weapons, it is necessary to understand how a laser propagates through a complex medium. For the U.S. Navy, the complexity of a maritime environment imposes particular challenges for laser propagation due to high concentrations of water vapor and high probabilities of liquid water in the form of fog, rain, or sea spray along the beam path. Although considerable research has gone into characterizing the maritime environment and simulating laser propagation through water vapor and turbulence, the interactions between a high energy laser (HEL) and liquid water are poorly understood. There are currently no physical or empirical models of HEL propagation through liquid clouds or sprays. Before a useful HEL spray model can be developed, the coupled interactions between an HEL and a single saturated (vaporizing) liquid droplet must be explored. The objective of the proposed work is to uncover the physical phenomena most responsible for controlling laser power and profile transmitted through single water droplets. Experimentation is required to elucidate both the thermodynamics and fluid dynamics in the droplet, and the effects that those thermofluid properties have on beam transmission.

A project is taking place in the United States Naval Academy's Directed Energy Research Center to investigate the interaction of a high energy laser and single water droplets. An HEL is used to irradiate droplets of water, and the droplet shape and size, the infrared radiation from the droplet, and the transmitted beam profile are measured and recorded. To control the droplet shape, it will be levitated using a commercial ultrasonic levitator, where the drop is held in place at a node by the pressure from a standing sound wave. Experiments will vary the drop size (initial diameter) and composition (salinity and turbidity). Both infrared and visible spectrum cameras off-axis captured images of the droplet as it is irradiated, facilitating modeling of the optical propagation, the resulting thermofluid effects on the droplet, and determination of time for vaporization. On axis, the beam exits the droplet into a beam profiler, which served to map out the irradiance of the beam, and how it varies over its cross-section. A combination of the heat maps from the beam profiler and the images from the cameras will provide a working knowledge of the effect the droplet has upon the beam as it is transmitted. Furthermore, multi-physics modeling tools will be used to help interpret and understand the experimental results.

The results of this experiment will provide an understanding of the coupled interaction between an HEL and a water droplet. Based upon these results, both offensive and defensive systems can be developed for distinct military applications. Analysis of the beam profile will provide insight into what configuration and number of droplets most effectively blocks directed energy. Similarly, the results can assist in determining when conditions are favorable for using a directed energy weapon, as well as when to expect cover from such attacks.

KEYWORDS:

HEL, Droplet, Vaporization Regime, Directed Energy, LaWS

TABLE OF CONTENTS

TABLE OF FIGURES

ACKNOWLEDGEMENTS:

INTRODUCTION:

High Energy Laser (HEL) weapons have been under development by the U.S. Navy and others as an alternative to conventional kinetic weapons. Lasers are a compelling technology due to their ability to reach their target quickly and engage many of the same targets as traditional kinetic systems, with the potential to exact a measured response, disabling or destroying as necessary [1]. Furthermore, they do not require ammunition in the sense of missiles or bullets; they only require electricity, which can be produced and harnessed at a fraction of the cost. A prototype system, the Laser Weapon System (LaWS), is currently in testing stages onboard the USS Ponce and is slated to be in operational use across the Navy by FY2021.

As LaWS comes closer to being a realistic shipboard asset, so does the reality of other countries possessing equal capabilities. The Chinese military has recently developed and tested its own laser weapon, Low Altitude Sentinel [2]. The Chinese system is designed to shoot down small drones in an urban environment at distances up to 1,500 feet. Able to burn through a drone in less than five seconds, this system is concentrated and powerful enough to cause structural damage to many targets [2]. Although far from the stage of being able to penetrate the skin of a maritime military vessel, this weapon is the first step in a laser program that looks to keep pace with U.S. naval weapons systems such as LaWS.

Perhaps the largest obstacle to the widespread use of laser weapons is their dependence on favorable atmospheric conditions [3]. In the maritime environment, high water vapor concentrations place limits on which types of lasers are useful, as some wavelengths are more susceptible to absorption than others. Most laser weapons, including LaWS, operate with an unpolarized continuous-wave beam at 1070 nm. The marine boundary layer creates fluctuations in the refractive index of the air due to thermal gradients and atmospheric turbulence, which induce fluctuations (scintillation) in the transmitted laser intensity [4]. Liquid water droplets from fog, rain, or sea spray are particularly problematic for transmission, and therefore directed energy weapons cannot at present be used in bad weather. On the defensive side, the observed challenges to laser weapons imposed by liquid water present an opportunity; it may be possible for a small watercraft or a drone over water to block a laser weapon with a spray of sea water.

The heating of a water droplet via HEL requires the synthesis of numerous scientific disciplines, such as heat transfer and optics. A starting point for the research project is the exploration of the experimental space, and a discussion of the relevant fields of study. Preliminary assumptions here are explored in depth to either confirm or deny validity of the experimental model. Experimental results are compiled in support of the engineering models presented in the following discussion, and their agreement is explored in order to develop the vaporization regime for large water droplets.

Laser Propagation and Geometric Optics

The irradiated droplets in this project will be characterized as "large," which means that the droplets are much larger than the wavelength of the light passing through them. Due to this fact, the interaction can be examined using geometric optics, also called ray optics, which makes for a simpler analysis that doesn't involve wave phenomena. Table 1 provides definitions of some common terms related to the propagation of electromagnetic radiation [5].

Term	Definition
Attenuation	Attenuation is the gradual decrease in magnitude of energy as the laser propagates through a medium
Refraction	Refraction is the change in direction of a ray as it passes from one medium into another
Reflection	Reflection occurs as a ray or object strikes a surface and is returned away from the surface rather than passing through
Absorption	Absorption is the removal of energy from a ray as it passes through a medium, where the energy removed from the ray is transferred into the medium
Scattering	Scattering is a wave phenomenon, which occurs as light strikes an object whose size is less than or equal to the light wavelength
Diffraction	Diffraction is defined as the bending of a wave around an object into the region of geometric shadow of the object

Reflection occurs when incident light contacts a surface and then leaves in another direction without entering or passing through the medium in question. Reflection may be either specular or diffuse in nature. Specular reflection occurs when the incoming rays are reflected in a single direction, whereas diffuse reflection results in oncoming rays being reflected in a variety of directions. Refraction occurs when a wave leaves one medium and enters another; for example, light refracts when it moves from air into water. Refraction is governed by Snell's Law (1), where n is the index of refraction and θ is the angle of incidence. The index of refraction is the speed of light in a vacuum divided by its speed in a particular medium, and varies from 0 to 1. Subscript "1" denotes the medium that light enters from, and "2" denotes the medium the light goes into after exiting the initial medium.

$$n_1 \sin \theta_1 = n_2 \sin \theta_2 \tag{1}$$

Thus, the end behavior of the ray depends not only on the angle at which it enters the new medium, but also the relative index of the new medium (See Fig. 1). Furthermore, the end state will change once more if the wave leaves the second medium back into the first. Due to their

spherical geometry, droplets can act as lenses, focusing energy inside the medium. Energy transmission through the medium is highly dependent on the shape of the interface.
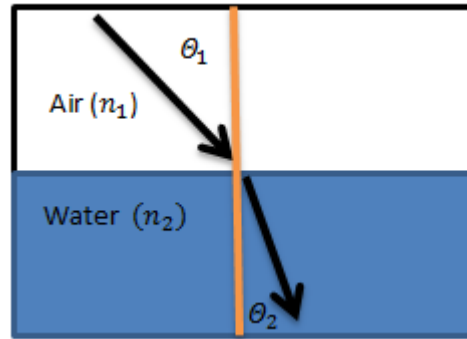

Figure 1: Refracted Ray

Lastly, absorption occurs when some of the electromagnetic energy is picked up, or absorbed, by the transmitting medium. Absorbed energy that falls within the thermal radiation band, like all visible and IR radiation, can serve to heat up the medium. Absorption can be described as an exponential decay using (2) known as the Beer-Lambert Law. Here, l_0 is the intensity of the incident ray, α is the coefficient of absorption, and x is the path length of the array as it travels through the medium. The variable l represents the intensity of the ray after it has propagated a length x through the absorbing medium.

$$l = l_0 e^{-\alpha x} \tag{2}$$

Absorption in water depends strongly upon impurities within the water being irradiated, and it is difficult to predict absorption for a given substance. Pure sea water consists of water and various dissolved salts, on the order of 35 parts per thousand by weight [4]. The salts in sea water have a negligible effect on absorption except at very long wavelengths. For IR radiation in sea water, phytoplankton is the primary particulate that determines optical properties, at lengths of 1 to 200 μm [4]. Chlorophyll and related pigments found in phytoplankton are strong absorbers of blue and red light, and thus contribute significantly to the absorption of light in sea water. Overall, the absorption of a water sample is highly dependent on its concentration of particulates like phytoplankton, and dissolved substances to a lesser extent.

Laser transmission will depend on the size and shape of the droplet, which will change as the droplet absorbs energy and vaporizes. The first law of thermodynamics states that the total energy within an isolated system remains constant; in other words, energy is conserved. Equation (3) is a basic form of the First Law of Thermodynamics, which governs the conservation of energy for a system. For a given substance, Q represents the heat transferred, W is the work developed and ΔH represents the corresponding change of the substance's enthalpy. In the case of a droplet, energy that is absorbed through radiative heat transfer will result in an increase in enthalpy. This rise in enthalpy will manifest itself either as latent or sensible heat. Sensible heat is heating that results in an increase in temperature. Latent heat is "hidden" heat, or heat that cannot be measured with temperature changes. Instead of increasing the temperature, the energy from latent heating is used to change the phase of the substance [6]. The enthalpy of

vaporization, H_{fg}, is the amount of energy required to change the phase of a material from liquid to vapor. The enthalpy of vaporization will vary based on temperature and pressure, but at standard conditions this is approximately equal to 2250 kJ/kg.

Vaporization occurs throughout a fluid when a saturated liquid is subject to continual heating. Evaporation differs from vaporization in that it occurs in unsaturated liquid phases, i.e., when the temperature is not at the boiling point. Evaporation occurs when an individual molecule at the liquid-air interface has reached its heat capacity.

$$1^{st}\ Law\ of\ Thermodynamics: \Delta H = Q - W \tag{3}$$

The heat Q in (3) may be determined from the heat equation, with a source term for heating by electromagnetic absorption and boundary conditions that account for both convection and radiation exchange with the surroundings. Work (*W*) refers to work produced by the system due to an energy transfer. In this vaporization interaction, no work is produced. Therefore, the change in enthalpy (*ΔH*) is a function of the heat transfer. The Heat Diffusion Equation (4) governs diffusion of heat in a solid or stationary fluid: $\tag{4}$

$$\frac{\partial H'''}{\partial t} = Q''' + \nabla * (k\nabla T)$$

where *k* is the medium's thermal conductivity, *T* is temperature, and each prime denotes per unit length. In (4), the leftmost term is the rate of change in enthalpy per unit volume. During the sensible heating phase this will relate to the increase in temperature of the medium, $\partial H / \partial t = mc_p\,\partial T/\partial t$. Once saturated, the enthalpy will continue to rise but cannot be related to temperature with a specific heat.

Related Work

The research proposed here involves rapidly vaporizing levitated water droplets using a Near-Infrared (NIR) high energy laser at 1070nm. A number of studies in the past have explored either the heating or vaporization of water by lasers, or the propagation of light through water. This work is unique because of its focus on the coupling of these phenomena; this project is focused equally on what the laser does to the droplet and on what effect the droplet has upon the laser. This project also differs from most of the previous work because of the inclusion of droplet levitation, the use of the 1070nm wavelength laser, and the size and variation of the water samples tested.

Droplet Effects

Previous research on droplet heating with lasers has usually used CO_2 lasers, which produce a 10-micron wavelength. The absorptivity of liquid water at this wavelength is much higher than at 1-micron, so heating effects can be drastic at the longer wavelength. The most interesting finding here was the discovery of two distinct heating regimes, a "slow" regime where the heat led to

rapid vaporization of the droplet and a "fast" regime where a single laser pulse resulted in explosive vaporization [7]. Because of comparatively low irradiance and the lower absorptivity of the light at 1.07-microns used in the experiments proposed here, all heating is expected to be in the "slow" regime.

Other work investigated the effects of irradiated droplets for the application of cloud clearance, using droplets with diameters from 2-100 μm and lasers of varying wavelength, from 1.06 μm to 10.6 μm [8]. This is considerably smaller than the droplet sizes intended for use in this project. An important consideration when working with droplets of this size was the speed of heating, with all vaporizations taking place in under one second. The slow-heating regime used by Armstrong and Park still resulted in a flash vaporization of the droplet [8]. Due to the increase in size, by orders of magnitude, the droplets in this experiment will vaporize much more slowly. Therefore, the explosive nature of vaporization documented by Armstrong and Park is unlikely to be replicated in this project.

Recently, combustion researchers interested in convective heating of spray fuels have used measurements of laser-heated, levitated water droplets to assess Computational Fluid Dynamics (CFD) models of fluid flow and heat transfer in and around ~1-mm droplets [9]. This work is relevant to the proposed work in that it demonstrates the feasibility of conducting fluid imaging experiments using levitated, irradiated droplets. The metrics in the CFD research were different, however, in that the droplets were doped with tracers, and the researchers measured the fluid flow inside the droplet but did not look at the downstream laser beam characteristics.

Lastly, some unpublished work presented at the APD-DFD meeting in November, 2014 examined the convective heating of droplets on substrates with different surface tension effects, which result in changes to the droplet shape [10]. The researchers found significant differences in the structure of the convection cells within the droplets based on the droplet shape. More spherical droplets with larger contact angles resulted in one circulation around a straight vortex line pinned at the edges of the droplet. Heating flattened droplets with smaller contact angles resulted in the formation of a horizontal vortex ring. Because the droplets in the research here were levitated, deviations from a purely spherical shape were much smaller. Nonetheless, changes in droplet shape and size affect the amount of energy absorbed from the laser as well as the convection profile. This is one of several modes of energy transfer in the droplet being explored.

Optical Effects

The propagation of light through a spherical medium with a different index of refraction is well understood. This occurs in, for example, the formation of rainbows when sunlight passes through water droplets in the air. Because of the droplet shape and its refractive index, lensing effects are important in these experiments – probably the most important factor in predicting the exit beam profile. Because this fundamentally depends on the droplet geometry, the exit beam profile then

depends upon the way this phenomena affects the thermodynamic processes described previously.

In the proposed experiments, absorption of laser light is of interest because of both the heating effects of the absorbed energy and because of the reduction in power of the exiting beam. For unpurified waters, absorption is dominated by the specific constituents present - suspended solid particles, algae, plankton, etc. [8] Because of this, predicting absorptivity of a given water sample can be difficult. Published literature provides some guidance on the expected range of property values, but effort is required to characterize the material-wavelength combinations of interest in the proposed experiments.

Other optical effects due to heating and phase change of the droplet are possible. The water vapor released from the droplet will need to pass through the path of the laser. Thus, there are effects from both water vapor and liquid water to take into consideration. Furthermore, convective heating of the air around the droplet may lead to increased scintillation. Nucleation and the formation of vapor pockets on impurities within the droplet may significantly alter the interior droplet geometry as well, resulting in additional deformation and refraction.

ONE DIMENSIONAL MODEL

To get a first approximation of the time scales required to vaporize water, the heat equation is applied here to a thin film for a one-dimensional model. As shown in Fig. (2), the fluid depth is the dimension of interest and can be regarded as the thickness that is irradiated by the laser. This model makes a host of additional assumptions including a uniform beam profile, infinite conductivity in the water, and insulated boundaries.
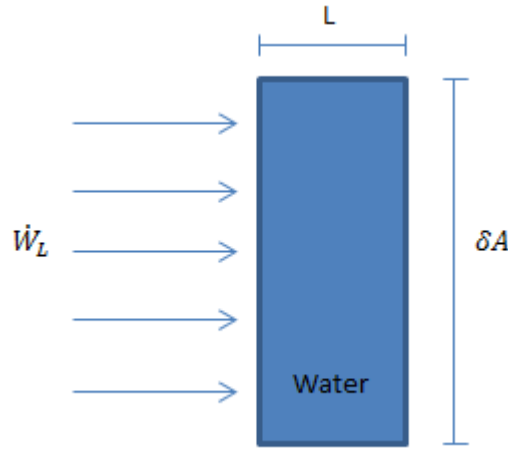
$$L = fluid\ depth$$

$$\delta A = differential\ area$$

Figure 2: Diagram of Irradiated Water

The irradiance will vary with path length and thus the final irradiance, after passing through the water, will be lower than the irradiance from the laser orifice. The following relationship (5) between irradiance and absorptivity can be used to model the irradiance upon the water droplet, and is simply an extension of the Beer-Lambert Law discussed previously:

Irradiance-Absorptivity Relationship:

(5)

$$I = I_o e^{-\alpha L}$$

$$I_o = initial\ irradiance\ (\frac{W}{m^2})$$

$$I = final\ iradiance\ (\frac{W}{m^2})$$

$$L = path\ length\ (m)$$

$$\alpha = absorptivity\ (m^{-1})$$

It follows that the power absorbed by the water is a fraction of the initial power radiated by the laser. The fraction of power absorbed per unit area is represented with the following relationship:

$$I_o - I = I_o(1 - e^{-\alpha L})$$

In this process, the water is vaporized by the irradiance from the incident laser. The term $\dot{W}_L$ represents the power from the laser upon the droplet. The heat of vaporization, h_{fg}, represents the energy required to change the phase of a liquid into a vapor. Here, it is represented on a specific basis, meaning that it is the energy required per unit mass. The heat of vaporization includes both the latent and sensible heat required for the water to change phase. As the area that is being irradiated changes, so does the rate at which the vaporization takes place. The energy balance of the water therefore has differential terms which account for the changing water depth as the vaporization takes place.

As derived previously, the heat equation is an adequate representation for the conservation of energy of a fluid. Here, the equation is expanded in greater detail for the specific application to irradiated water. First, since a phase change is occurring, the leftmost term as stated above is inadequate in describing the change in energy for the water. Therefore, the change in size during phase change and the specific enthalpy of vaporization must be taken into account. Shown below is the transformation of the leftmost term to reflect these parameters.

$$\frac{\partial H}{\partial t} = -h_{fg}\frac{\partial m_{water}}{\partial t} \approx -h_{fg}\rho \delta A \frac{dL}{dt} \tag{6}$$

The first term on the right side of the equation pertains to heat transfer via conduction. We assume a uniform temperature in the thin film, and this this term falls to zero. The second term, *S,* is the unique source term for the given application. For this project, the source term is derived from the Beer-Lambert Law (2). When accounting for the negligent heat conduction through the film and the source term, we can adjust the heat equation (4) for the specific purpose of modeling the vaporization of an irradiated film of water.

Due to uniform temperature assumption: $\nabla * (k\nabla T) = 0$

Source term for incident laser energy, from Beer-Lambert Law: $S = \delta A I_0(1 - e^{\alpha L})$

$$I_0(1 - e^{-\alpha L})\delta A = -h_{fg}\,\rho\,\delta A\,\frac{dL}{dt} \tag{7}$$

$$(Power\ absorbed\ from\ laser) = (Rate\ of\ Vaporization)$$

In differential form: $\quad \frac{dL}{dt} + \frac{I_0}{\rho\,h_{fg}}(1 - e^{-\alpha L}) = 0$

To demonstrate the relationship between the thickness of the water and the time it takes to fully vaporize it, an absorptivity of 14.8 m^{-1} is used. This is the absorptivity of pure water at a wavelength of 1069 nm, which is close to the wavelength of the laser to be utilized in this

experiment [8]. Even using the simple 1-D model, the system is described by a non-linear differential equation. A numerical solution with the following parameters can be used to deduce the approximate half-life and time for complete vaporization of a water sample when solved with the Euler method.

Numerical Solution:

The differential form of the heat equation as applied to this project was solved using the Euler method, and plotted in MatLab to give a sense of the timescale and general behavior of the film as it is irradiated. The solution is plotted on the next page, using the following parameters:

Table 1: 1D Model Parameters

L_0 (Initial path length)	1 mm
α (absorptivity)	14.8 m^{-1}
P (density)	1000 kg/m^3
h_{fg} (enthalpy of vaporization)	2256 kJ/kg
I_0 (Initial Irradiance)	509 W/cm^2
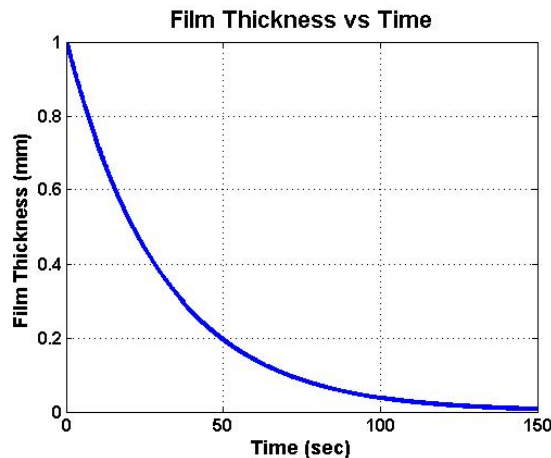
Figure 3: Water thickness as a function of time

From Figure 3, the greater the thickness of the water, the greater the rate at which it vaporizes. Though not an exponential curve, the relationship does follow an exponential trend, and it is useful to relate the rate of vaporization to exponential decay. The half-life denotes the time it takes for half of the mass of a certain substance to decay, and remains the same despite the initial amount of the substance. As shown in the graph, the approximate time to vaporize half of the water and decrease the fluid depth to 0.5 mm is approximately 21 seconds.

There are several ways in which this model will be improved by the experimental data collected through the course of this project. In the one-dimensional model, it is assumed that the laser heats the film uniformly. Due to the curvature of the droplet, there will be uneven heating in the

droplet. Experimental measurements thus far have not provided much insight into the temperature profile within the droplet. This will allow either for the incorporation of non-uniform heat deposition, or the use of geometric optics coupled with basic thermodynamic principles to illustrate the effects of uneven heating.

The second major contribution of the experimental data to the model is the effect of the water vapor after vaporization has begun. In the one-dimensional model, it is assumed that mass is transferred from the thin film by release of saturated vapor from the surface, leaving only a film of reduced thickness. In reality, there will be water vapor present after the water has begun to vaporize. IR measurements will show the effect of mass transfer from the droplet to the surrounding air, and how this transfer affects the laser's propagation through the droplet and surrounding air.

Lastly, the one-dimensional model does not account for the fact that the droplet will be suspended in an acoustic standing wave. It is unclear exactly how the pressure nodes from the standing wave will affect the energy or mass transfer, but experimental results will allow for the observation of their effects. These could include enhanced mixing, and therefore a more homogenous thermal profile within the droplet, or deformation and instability within the droplet as it decreases in size.

Experimental Equipment:

All experimentation took place in the Naval Academy's Directed Energy Research Center (DERC), a facility built over the last eight years that has support and supports several directed energy projects through the Office of Naval Research (ONR), the HEL-JTO (High Energy Laser-Joint Technology Office), and the Academy's Division of Engineering and Weapons. The DERC contains most equipment be necessary for this experiment, including three high energy lasers, a beam profiler, ultrasonic levitator and various types of cameras. Other items, such as a Jasco V-670 Model Integrating Sphere and micropipette, are located nearby in the chemistry department at USNA. All of the requisite equipment is currently on-site and functional.

The experiment itself will involve levitating water droplets and then using the laser beam to vaporize them. Figure (4) shows a schematic of the overall experimental setup. Labeled components will be discussed in greater detail on the next page.
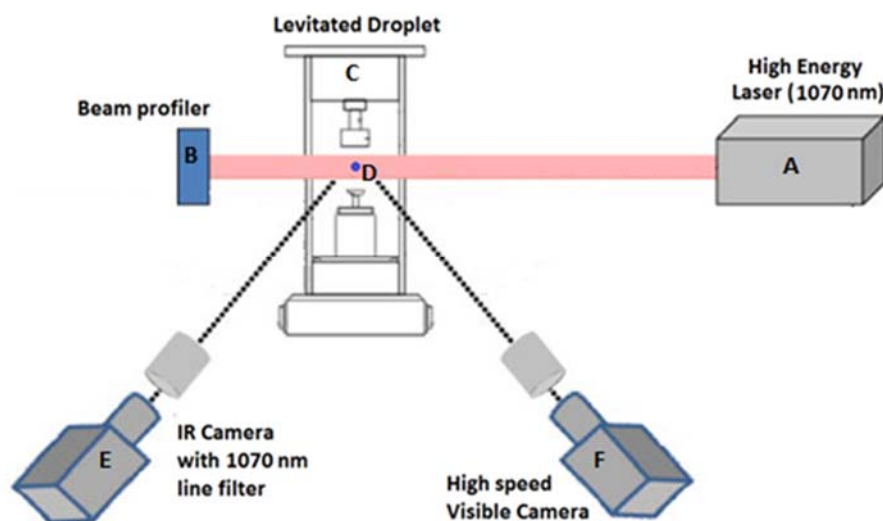
Figure 4: Setup Schematic

A. High Energy Laser

The laser used in this experiment is a 100-W IPG High Power Fiber laser. The laser has a spot size of approximately 5 mm and a wavelength of 1070 nm. With a nominal power of 100 W and a beam diameter of 5mm, this laser delivers an irradiance of 509 W/cm^2. It can be run continuously in steady-state operation indefinitely [11]. The laser is one of three of its kind at the laboratory, and thus can be replaced if any sort of breakdown or malfunction were to occur. The laser and all test equipment is housed to protect against scattered laser light.
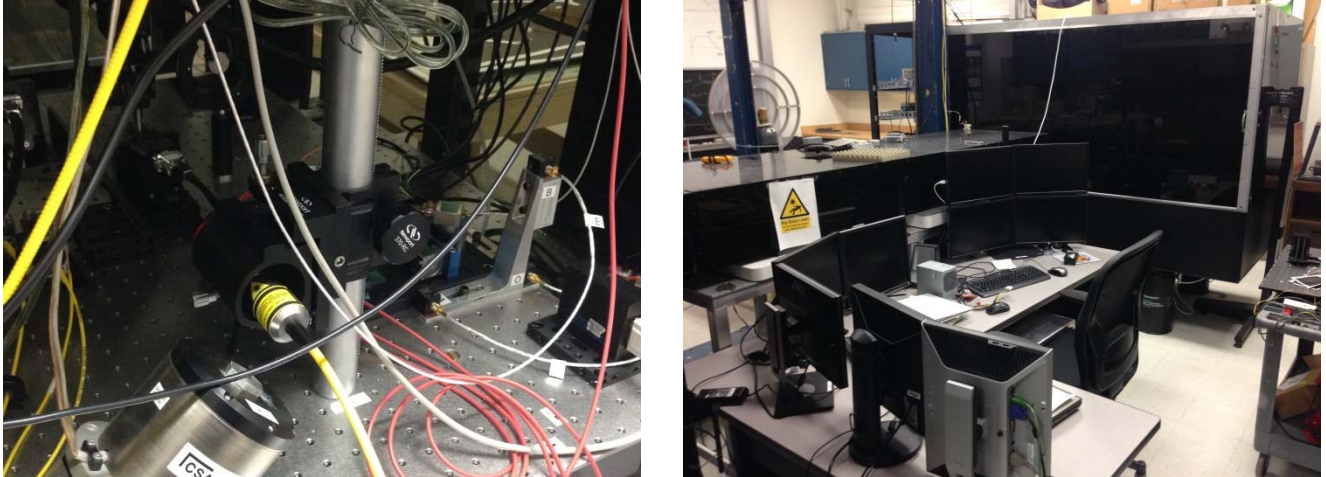
Figure 5: HEL (left) and protective casing (right)

B. Beam Profiler

 The beam profiler is a combination of beam cube and attenuator, which will measure the energy of the laser that passes through the droplet. The sensor has a 1600 x 1200 pixel resolution, and is capable of 7.5 frames per second at full resolution. The beam profiler will provide an idea of how much radiant energy is able to make it through the droplet, and will show how this amount changes in time as the droplet is vaporized.

.

Figure 6: Beam Profiler

C. Ultrasonic Levitator

The droplets in this experiment were suspended by a tec5 AG ultrasonic levitator. Standing sonic waves were used to suspend the droplets and hold them in place for the laser beam to irradiate. This levitator produces 4 to 5 pressure nodes at which forces are equalized, but only 2 to 3 can be used for stable levitation [8]. The size of the droplets levitated is dependent upon the wavelength

of the sonic wave being used to create the pressure nodes. The optimal droplet diameter is given as $d_s=\lambda/3$, as this is the diameter that requires the minimum power to levitate the droplet. The standard operating parameters for the levitator are a wavelength of about 5.9 mm and a frequency of 58 kHz [8]. Thus, the optimal droplet size would be approximately 2 mm. In these experiments, droplet size did not exceed 2.5mm, using mid-rnage power while creating a stable platform for droplet levitation. The acoustic energy density profile surrounding the levitated droplet causes the droplet to deform and take on an oblate spheroid appearance. This is a result of the balancing of capillary and gravitation forces experienced by the droplet during its levitation.
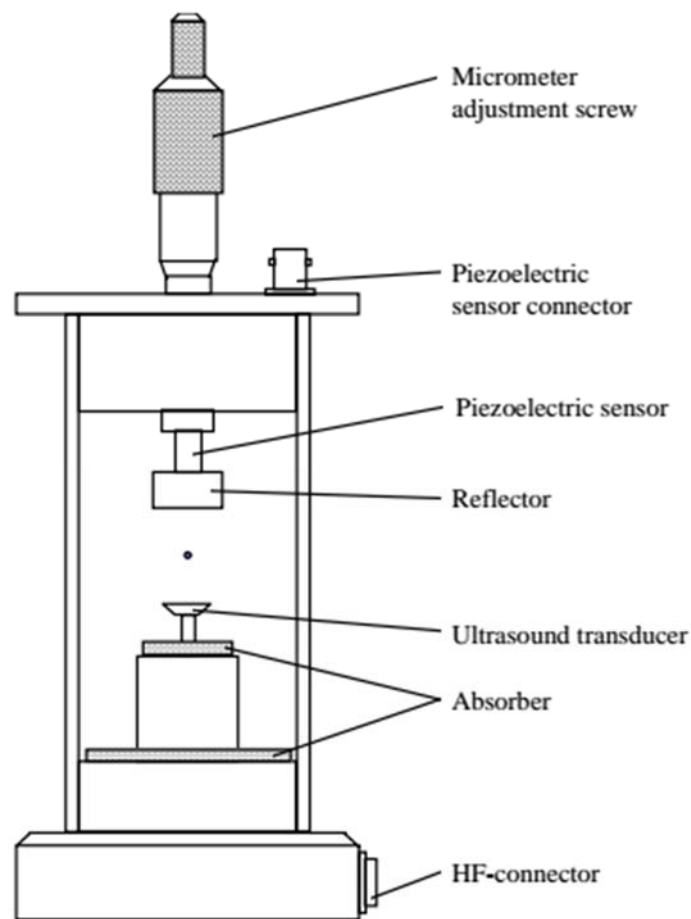
.

Figure 7: tec5 Ultrasonic Levitator Schematic [8]

D. Levitated Droplet

The irradiated water will be a droplet about 1 mm in size. The majority of experiments will be conducted on droplets of distilled water, though some testing will be done on droplets of salt water as well. Salt water causes more attenuation in the light beam due to a higher density of

dissolved particles and particulates, but these imperfections in the droplet do not significantly affect the absorption of the laser energy, only its scattering [4].
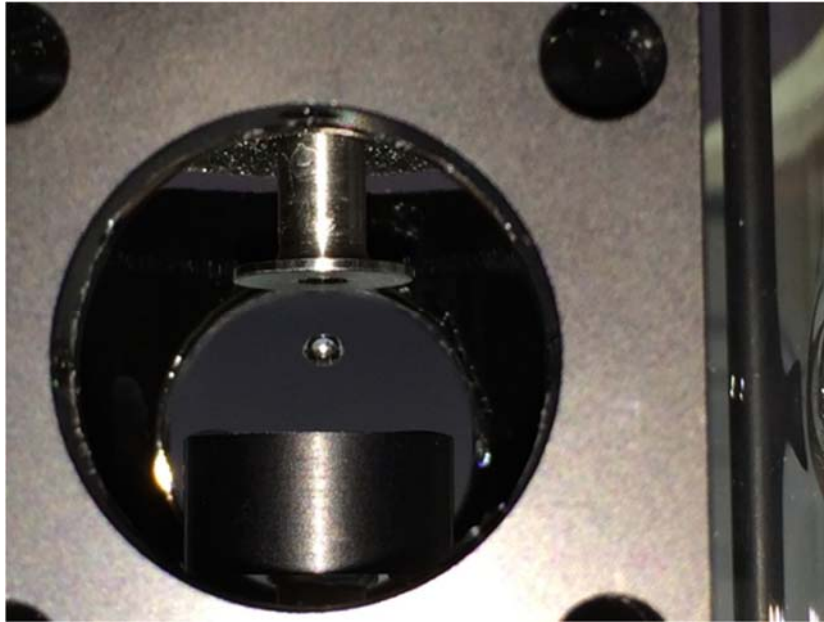

Figure 8: Droplet suspended in Ultrasonic Levitator

E. High-Speed Visible Camera

The Hamamatsu ORCA-Flash2.8 is a high-resolution, 45 fps visible spectrum camera has been used previously in the DERC, and is the primary data collection for these experiments. An additional lens, in the Navatar 6000 series, was recently acquired that will allow for better resolution and larger droplet imaging. This will be useful in analyzing the test matrix for next semester. The prior camera setup utilized a standard Navatar 7000 series lens configuration which performed adequately. The images captured from the original setup were used in all data analysis from the first half of the experiments.

In addition to the equipment shown in the schematic, a Jasco V-670 Model ISN-723 integrating sphere was used to determine absorptivity for the water samples tested over the course of the semester.

BEAM CHARACTERIZATION

The goal of these experiments is to explore the coupling that exists between the interaction of an HEL and a water droplet. To do so, the beam must be adequately characterized in order to provide an accurate picture of the energy that is received by the drop.

The IPG Ytterbium doped Yttrium Aluminum Garnet (Yb:YAG) fiber laser used in these experiments has a nominal 100W power output over a nominally Gaussian distribution. The maximum $1/e^2$ beam diameter, as measured by the manufacturer, is 5.5mm and results in an average irradiance of approximately 500 W/cm^2. An electromagnetic beam such as this has

infinite width but rapidly diminishing profile. The $1/e^2$ value of the peak of irradiance is used as the industry standard for beam radius [12].
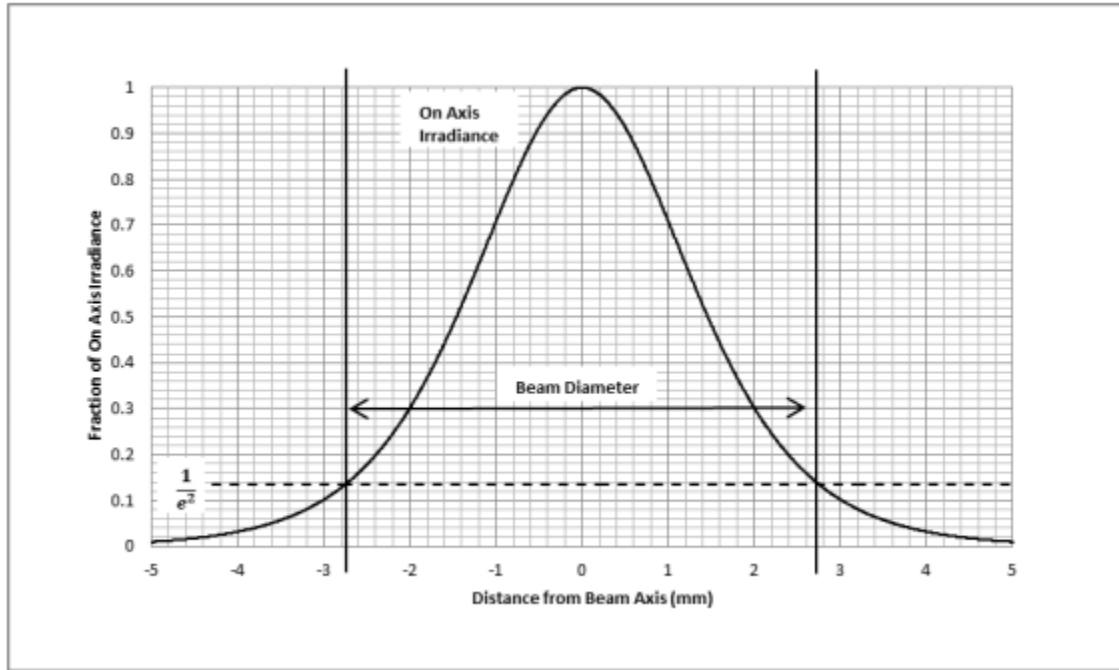

Figure 9: Measurement of $1/e^2$ beam radius

The average $1/e^2$ for this particular laser is 5mm, and therefore the beam diameter is referred to as 5mm. True energy distribution was tested using the BeamGage due to the small target size of the droplet.

Although the Graphical User Interface (GUI) used to run the laser has input values for nominal power, it was important to determine the actual power delivered to the drop. To do so, the expected power from the laser compared to the actual power received by the thermopile for several nominal values. These tests were run without a droplet so the beam could pass unimpeded from the source to thermopile.

The measurement of actual power delivered on target also allows for the analysis of the droplet's effect on the beam and its profile. The thermopile and BeamGage were used in conjunction with each other to determine the baseline operation of the laser. The thermopile collected raw power, and the BeamGage provided an accurate representation of the energy distribution across the beam's cross-section. Provided below is a representative beam profile and average values of the relevant parameters used to define the power density distribution.
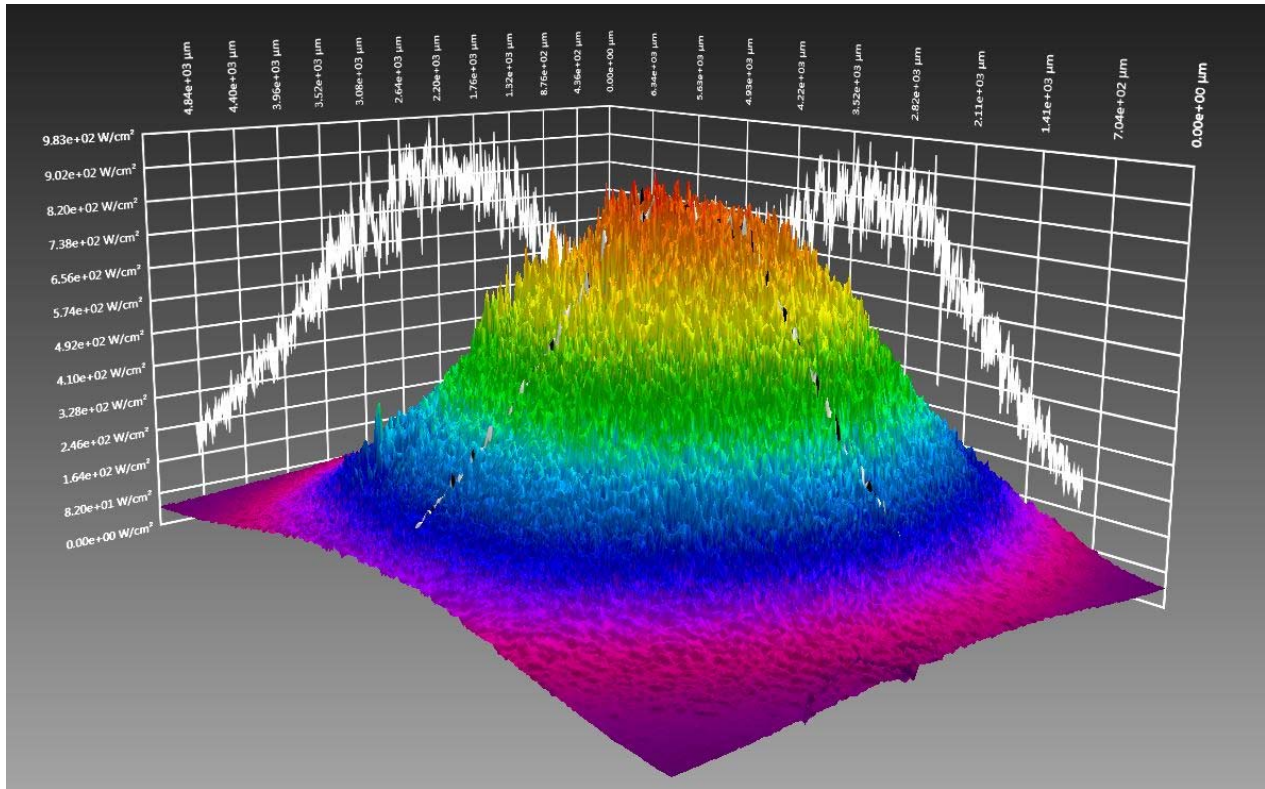
Figure 10: HEL in BeamGage

Parameters collected from the BeamGage were used to determine the radiation distribution. The laser has a nominally Gaussian distribution, so the data collected was used to fit a three-dimensional surface using the following equation for a normal distribution in three dimensions.

$$J(x,y) = \frac{1}{2\pi\sigma_x\sigma_y} e^{-(\frac{(X-u_x)}{2\sigma_x^2} + \frac{(Y-u_y)}{2\sigma_y^2})} \tag{7}$$

Table 2: HEL Variables

Variable	Significance	Value (from BeamGage)	Units
X	Variate 1	-2.64<x<2.64	mm
Y	Variate 2	-2.64<y<2.64	mm
σ_x	Standard deviation in x	1.1395	mm
σ_y	Standard deviation in y	1.1813	mm

Using the average parameters collected from the BeamGage, the distribution has been plotted and is shown below. This distribution has been used as a baseline of energy deposited upon the droplet. In conjunction with ensuing experiments including a levitated drop, it provides the maximum amount of energy that may be incident upon a droplet of a shape and size. Experimentation across a range of power operating levels, from 25W to 100W, has proven that this distribution remains the same. Therefore, it can be used to compare the beam as it passes unimpeded to the cross section after it has encountered a water droplet within the levitator.

Table 3: Power tests over range of system capability

Nominal Power [W]	Actual Power [W]	% Difference
100	107.0	+7.0%
75	77.2	+2.9%
50	49.1	-1.8%
25	20.0	-20%

The purpose of the power test was to determine the actual power delivered so that calculations involving the irradiance from the laser source were accurate. True power is higher than nominal power across the range of testing.

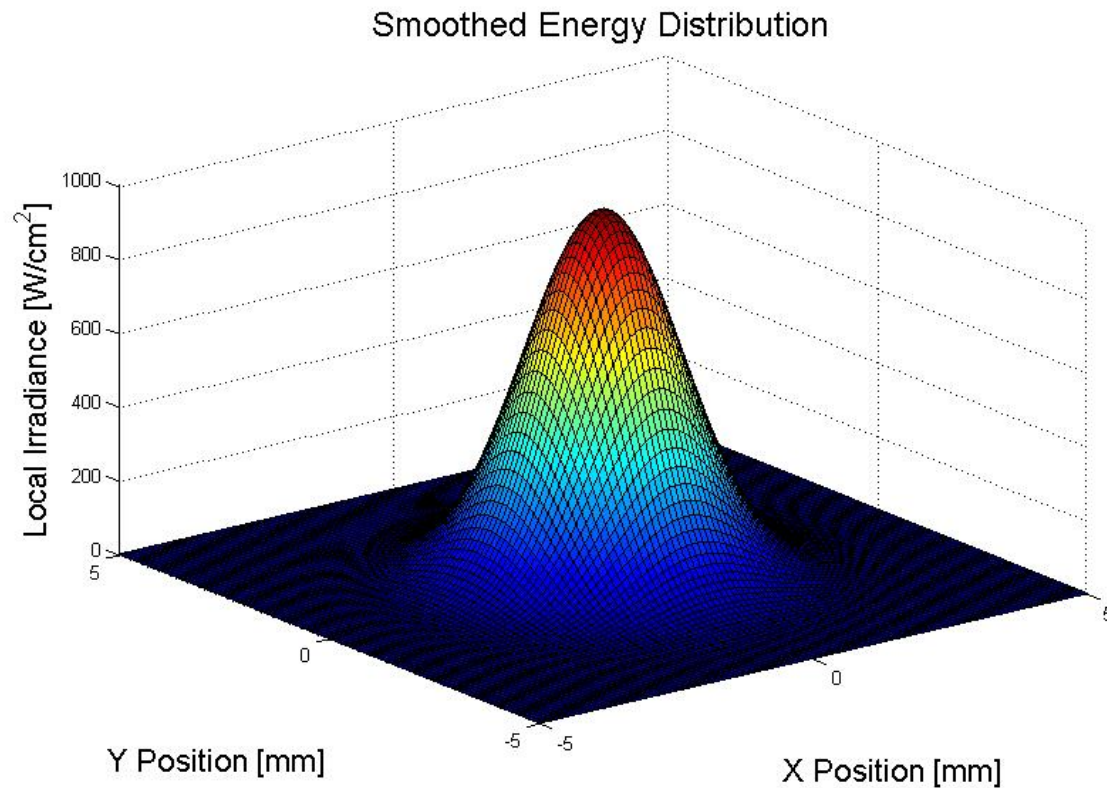Figure 11: Smoothed Gaussian Distribution

By adjusting the aperture of the BeamGage, the percentage of the total energy captured was calculated for the unimpeded beam. This was done to establish a baseline to compare to the profiles after the beam had interacted with a droplet. Table 4 shows the percentage of energy collected for each aperture size, all the way to the maximum aperture of 5.280 mm.

Table 4: Energy deposited in BeamGage Aperture as Function of Aperture Size

Aperture Diameter (mm)	Percentage of Energy Contained	Aperture Diameter (mm)	Percentage of Energy Contained	Aperture Diameter (mm)	Percentage of Energy Contained
0.2	0.21	2.0	19.6	3.8	56.77
0.4	0.85	2.2	23.3	4.0	60.91
0.6	1.9	2.4	27.2	4.2	64.92
0.8	3.35	2.6	31.27	4.4	68.82
1.0	5.18	2.8	35.45	4.6	72.45
1.2	7.4	3.0	39.71	4.8	75.69
1.4	10.0	3.2	44.01	5.0	78.65
1.6	12.92	3.4	48.3	5.2	81.97
1.8	16.14	3.6	52.56	5.28	83.11

ASSESSMENT OF 1-D MODEL
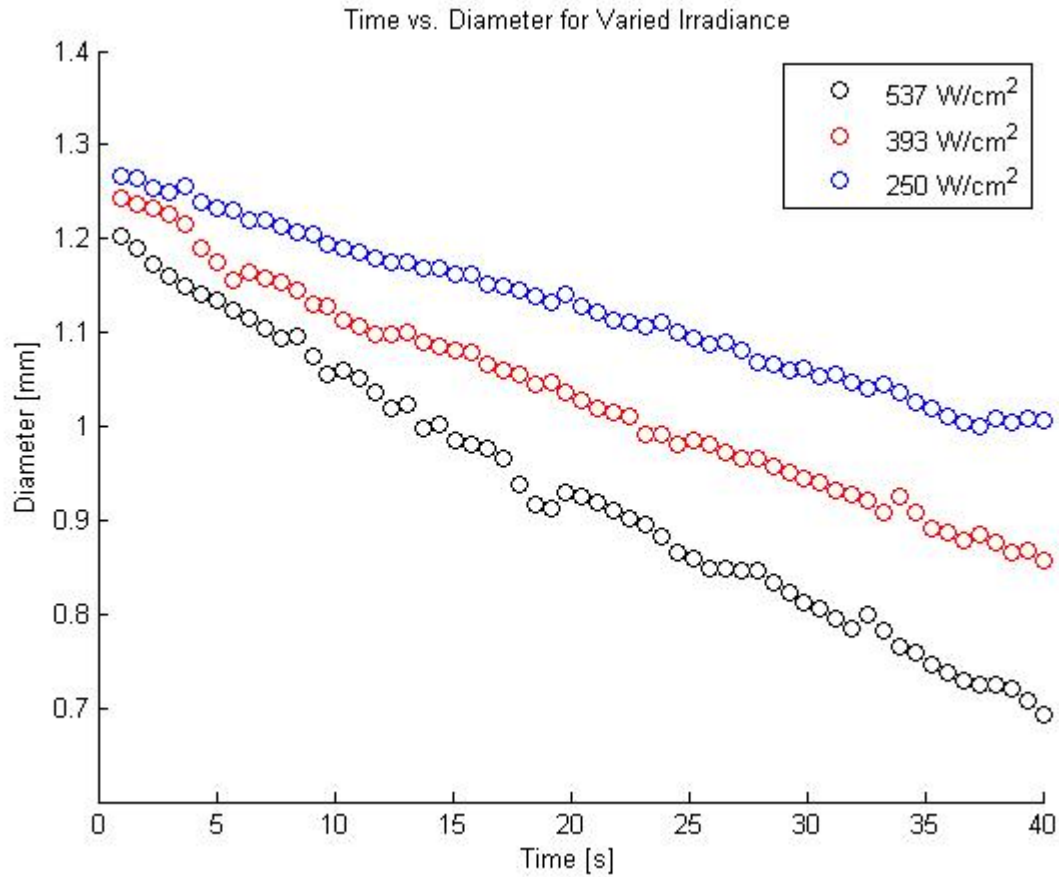
Figure 12: Effect of Irradiance on diameter changes

As evidenced by Figure 12, the vaporization rate decreases with lower irradiance.

The following results have been collected to demonstrate repeatability of the experiment and glean insight into the composition of the future testing matrix. The laser setup characteristics for the droplet runs shown here are located in Table 3.

Table 5: Laser Setup for Variable Volumes

Parameter	Value
Laser Power [W]	100
Time [s]	40
Irradiance [W/cm^2]	537

As previously discussed, the nominal laser power of 100W corresponds to an actual power received of approximately 107W. This value is reflected in the irradiance of 537 W/cm^2.

The first item of interest in the experiment was agreement with the 1D model results presented in Figure 3. The 1D model made several simplifications to the actual experimental setup, accounting for only major parameters. Figure 15 shows a comparison of representative experimental data with the model results.
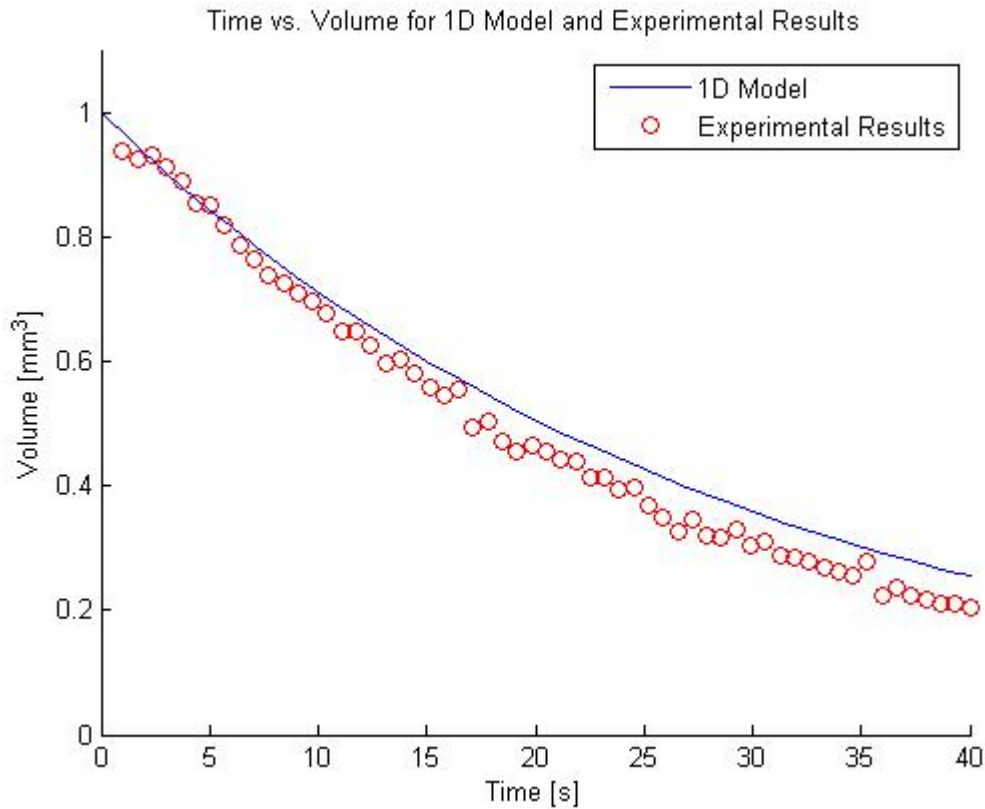

Figure 13: Comparison of 1D Model to Experimental Results

As seen in Figure 13, the results of the 1D model and experimental agree well. The model assumed a change in thickness coupled with a differential area that stayed consistent over the course of the irradiation. This of course was not the case in the experiment, as both geometry and operating conditions were different. The results suggest that absorptivity and laser power are the driving factors that affect volume change for the droplet. Geometry may still prove to be important to the vaporization rate, but this data suggests that it is not as important as the relative size of the droplet. The good model fit also suggests that concerns about the effects of the acoustic wave on phase change were unfounded.

The same experimental data set was used to find a representative half-life for droplet volume. In Figure 16, the experimental data is shown with the polynomial best fit. From the best fit line, the half-life was determined. Here, half-life is defined as time required for a 50% reduction in size.
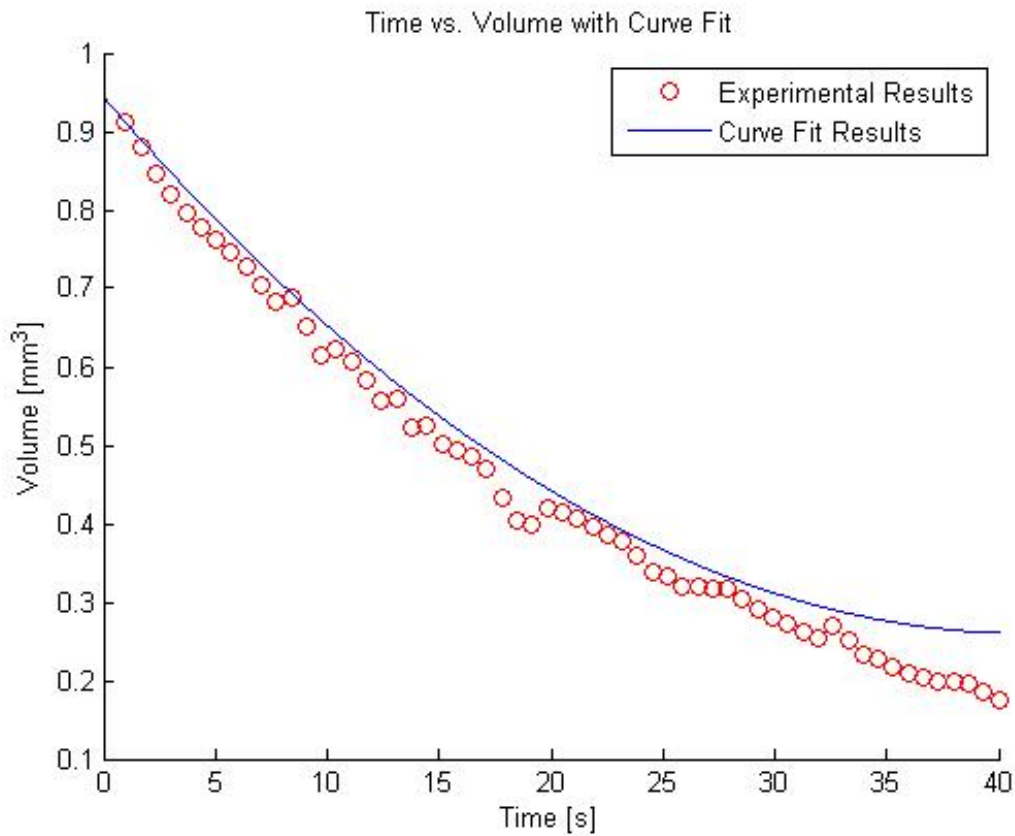

Figure 14: Fitted Line with Experimental Data

The half-life determined from the best fit line was 18.3 seconds. The 1-D model returned a larger half-life of 21 seconds. This is consistent across other runs conducted at the same droplet size. The polynomial fit of the data agrees through 30 seconds of run time, but later in the interaction it becomes less accurate. The interaction can be loosely approximated by a polynomial fit, but the governing physical processes follow a different trend.

One of the primary purposes of the testing conducted this semester was to provide concrete baselines and establish the repeatability of the experimental procedure used to collect data. Initial tests were frequently poor, with droplets being lost in the middle of vaporization. As the testing scheme was improved, the corresponding change in quality of collected data proved to be significant. Experiment repeatability is demonstrated in Figure 17, which shows multiple runs at the same pipette setting and their subsequent results for change in volume. Figure 18 illustrates the same concept at a different pipette setting.
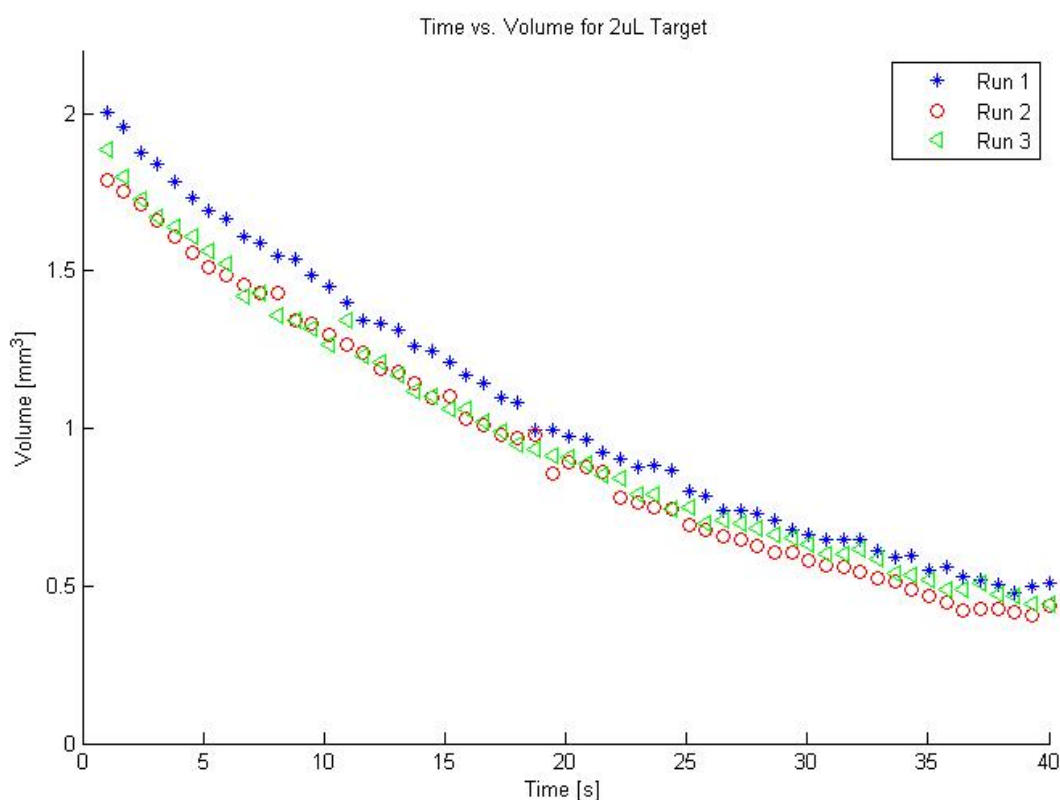
Figure 15: Repeatability at Pipette setting of 2uL

The results shown in Figure 15 are important in several ways. First, they verify that the trend remains consistent from run to run, with the biggest difference coming from initial droplet size. The micropipette used for the experiments is significantly better than the syringe that had been used earlier in the year, but is still lacking in precision. Experimentally, the volume varied by approximately 10% from run to run. However, the droplet size is accurate and results show that one run is representative of the behavior of other runs within its immediate vicinity of droplet size. This will be helpful going forward, as a wide range of droplets can be tested and any

anomalies spotted can quickly be investigated with confidence that there are relevant physical phenomena rather than experimental noise.

Figure 16: Results for 1.5 uL setting

Figure 16 reinforces the consistency of the results in presented in Figure 15, but also illustrates the presence of outliers within the data set. A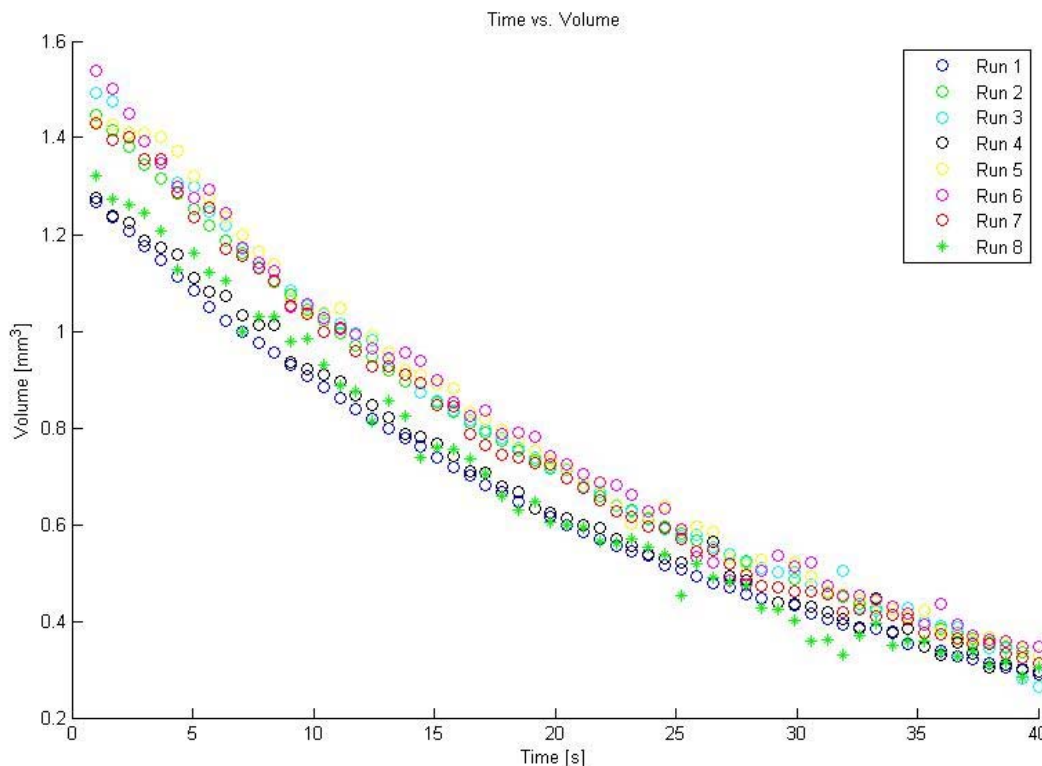s mentioned in the discussion of image analysis, it is not uncommon for the droplet to move slightly while being irradiated, and slight changes in shape result in different reflection of visible light that can result in false diameter readings. Run 6 and Run 2 illustrate the most notable of these outliers. The experimental trend remains largely the same regardless; this much data presented at once can be difficult to interpret, but this figure is important in reinforcing that one run can be used to generate meaningful data interpretations. Some data sets are obviously wanting, such as Run 2. The diameter of zero is the result of an unsteady droplet being lost from the levitator. There could be several reasons for this, which are discussed later on.

The first observation that stuck out in the data analysis was the almost immediate reduction in droplet size. This suggests that the period of sensible heating is quite brief and the vaporization process begins rapidly. These observations were for an irradiance of approximately 510 W/cm^2, which is the maximum irradiance achievable in the laboratory. An energy balance was conducted on the droplet to determine the irradiance required to begin phase change.

NUMERICAL MODEL

In order to develop a better understanding of the HEL-droplet interaction an energy balance was conducted on a water droplet. In its most basic form, the interaction of laser energy with a single droplet involves incident energy, which is then transmitted, reflected or absorbed in the mass itself. Because the spot size of the HEL used in this experiment is 5mm, much larger than any droplet studied, there will also be some energy that passes to the beam profiler unimpeded.

$$Laser\ Irradiance\ (G) = Incident\ Energy + Unimpeded\ Energy$$

Incident energy is the total energy that interacts with the droplet and takes part in the coupling between droplet and HEL. Unimpeded energy passes from the laser aperture to the beam sink without interacting with the droplet. The HEL was tested using the BeamGage, which resulted in data showing both total energy captured for a certain aperture size, as well as the distribution of energy across the beam's cross-section.
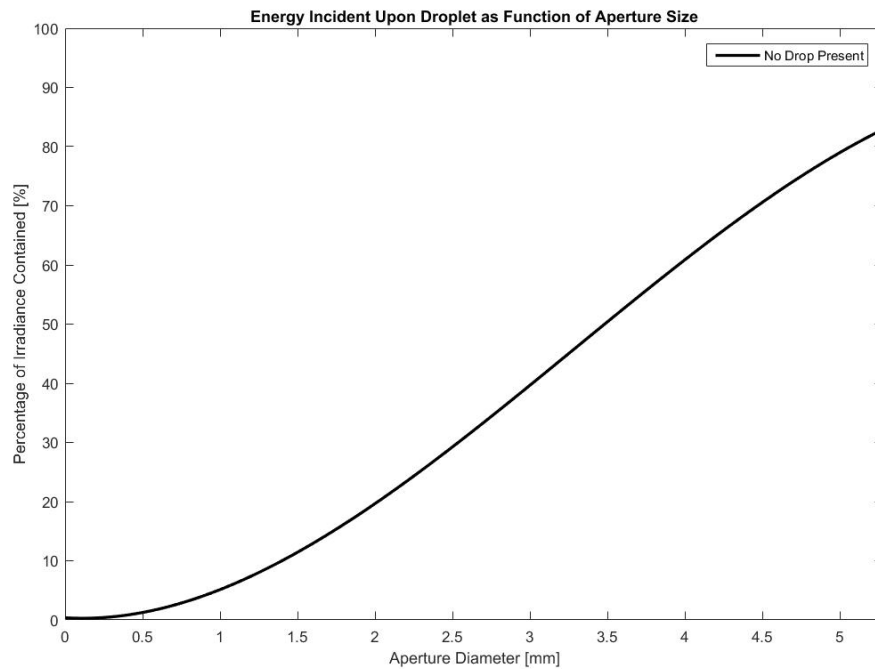

Figure 17: Energy Incident Upon Droplet as Function of Aperture Size

From the beam profile, the amount of energy that actually interacts with the levitated droplet can be quantified. The amount of incident energy can then be split into the different modes of dissipation from the droplet.

$$Incident\ Energy = Reflected + Transmitted + Absorbed$$

The majority of the energy provided by the HEL does not directly contribute to the droplet decay. A large portion of the energy is transmitted and passes through the droplet without interacting with the water molecules. Additionally, the surface of the droplet provides ample opportunity for the incoming light to be reflected rather than absorbed. Only a small fraction is absorbed, which is a function of both the droplet size and the absorptivity of the water sample.

The energy absorbed by the droplet is largely dependent on the absorptivity coefficient of the sample. Absorptivity is a measure of the amount of radiation absorbed by the sample at a given wavelength. Because the HEL operates at 1070nm, an experiment was conducted using a Jasco Near-Infrared Spectrometer. The results of the spectroscopy were used to determine the absorption coefficients for all water samples.

Energy that is absorbed by the water droplet is then released by one of several modes. The energy may be radiated back to the surroundings, dissipated through convection between the droplet surface and surrounding air or released through mass transfer. Because the droplet is stationary, free convection is assumed. Although forced convection drives transfer within the droplet itself, there is no external forcing agent that causes significant flow in the air surrounding the droplet. Therefore, free convection correlations are appropriate for use in determining the heat transfer coefficient. Assuming that the energy into the system (energy absorbed) is equivalent to energy out of the system (energy dissipated), the following balance governs the exchange between the droplet and its surroundings.

$$Energy\ Absorbed = Energy\ Dissipated$$

$$Energy\ Absorbed = q_{rad} + q_{conv} + q_{mt}$$

Under steady state conditions, the surroundings are isothermal. The droplet area is much smaller than the area of the surroundings, and thus the droplet may be approximated as a blackbody. The droplet has an emissivity of ε_s and Temperature T_s. The radiation balance accounts for the exchange between the shield surrounding the experimental apparatus and the droplet.

$$q_{rad} = \varepsilon \sigma A(T_s^4 - T_{surr}^4) \tag{8}$$

The basic form for the convection exchange is governed by Newton's Law of cooling, which states that the rate of heat transfer is directly related to the difference in temperature between the bodies involved in the exchange. The heat transfer coefficient accounts for the nature of the bodies involved.

$$q_{conv} = \bar{h}A(T_s - T_{surr}) \tag{9}$$

In order to determine the average heat transfer coefficient, $\bar{h}$, the Nusselt number is used [13]. Due to geometric considerations, the Nusselt correlation for a sphere is used to satisfy equation 10.

$$\overline{Nu}_D = \frac{\overline{h}D}{k} = 2 + \frac{0.589 Ra_D^{1/4}}{[1+(\frac{0.469}{Pr})^{9/16}]^{4/9}} \tag{10}$$

The correlation for the Nusselt Number is dependent on the Prandtl and Rayleigh numbers, Pr and Ra_D. The approximation in equation 10 is valid so long as Pr> 0.7 and $Ra_D < 10^{11}$. Under steady state conditions, both of these requirements are satisfied. The Rayleigh number is determined using the free convection correlation for a sphere and represents the effect of buoyancy-driven flow, or natural convection taking place due to temperature difference.

$$\overline{Ra} = \frac{g\beta(T_s - T_{inf})(d/4)^3}{\nu(\frac{k}{\rho c_p})} \tag{11}$$

All property values are taken at T_f, the film temperature, which is defined as the average of the surface temperature and ambient temperature. The Churchill correlation for Nusselt number and the Rayleigh correlation were used to solve for $\overline{h}$.

The final major mode of energy dissipation occurs in the form of mass transfer from the droplet. Once the droplet reaches sufficient temperature to begin boiling, water vapor is released from the droplet surface. Equation 12 describes the basic process of mass transfer from the liquid droplet to water vapor in the surroundings.

$$q_{mt} = \rho h_{fg} \frac{dV}{dt} \tag{12}$$

The physical process of mass transfer is more complex than illustrated here, but at its most basic, the energy required to induce sustained phase change is related to the enthalpy of vaporization of the substance.

To induce vaporization, the energy absorbed by the droplet must be greater than the sum of the energy dissipated by convection and radiation under the initial conditions. Here, the initial power required to initiate phase change is found by applying the energy balance calculations to a droplet 1mm in diameter. Increased irradiance is then manifested through an increase in the decay rate, dV/dt.

Table 6: Conditions to Initiate Phase Change in 1mm droplet

Parameter	Description	Value
G [W]	Power from laser	Unknown
d_o [m]	Initial Droplet Diameter	0.001
A_f [m^2]	Droplet Cross-Section (for d=0.001)	7.853 x10^{-7}
A_b [m^2]	Beam Cross-Section	1.963 x10^{-5}
A [m^2]	Surface Area of Droplet	3.1415 x10^{-6}
α [unitless]	Absorptivity	0.14
ε [unitless]	Emissivity	0.96
σ [W/mK^4]	Stefan-Boltzmann Constant	5.67 x10^{-8}
v [m^3/kg]	Specific Volume	0.001044
ρ [kg/m^3]	Density	957.85
T_s [K]	Surface Temperature	373.15

T_{surr} [K]	Temperature of Surroundings	294
T_{infinity} [K]	Ambient Temperature	295
cp [J/kg*K]	Specific Heat	4217
Pr [unitless]	Prandtl Number	1.76

By applying the initial conditions shown in Table 6, the initial power required to initiate phase change is calculated. The following are the results when taking into account the effects of radiation and convection.

Table 7: Calculated Values for Phase Change Initiation

Parameter	Description	Value
Ra [unitless]	Rayleigh Number	12.46
Nu [unitless]	Nusselt Number	2.93
h [W/m²K]	Heat Transfer Coefficient	1993.10
q_{rad} [W]	Power Dissipated by Radiation	0.0079
q_{conv} [W]	Power Dissipated by Convection	1.8772
q_{mt} [W]	Power Dissipated by Mass Transfer	0

$$Energy\ Absorbed = q_{rad} + q_{conv} + q_{mt}$$

$$0.0079\ W\ (radiation) + 1.8772\ W\ (convection) + 0W\ (mass\ transfer) = 1.8851\ W$$

The power required to initiate phase change is only 1.89 Watts. For a power setting of 100W from the HEL, the incident power absorbed by the droplet is 4.72 W. This accounts for the absorptivity of the sample as well as the profile of the beam. It is assumed that this remaining power directly contributes to the phase change of the droplet. The next step in understanding the coupled reaction is relating this excess energy and how it manifests itself in the decay of the drop over time.

DATA COUPLING

The two main sources of data collection, in the form of the beam profiler and high speed camera, are most meaningful when viewed in reference to one another. Data is presented here in such a way as to emphasize the effects of the droplet upon the beam, and well as the changes in the droplet itself. Results for a specific power setting and diameter are shown and discussed in order to develop trends across the range of experimentation while keeping focus on the intertwined nature of the results.

The first section of data coupling contains the data from all data sources used during experimentation. Power readings from the power meter give the total power that passes through the testing apparatus, and the BeamGage provides more exact information with regard to the cross-sectional intensity of the beam. The results for the BeamGage are taken from the beginning of the beam vaporization. This is due to the high memory requirement for the BeamGage data collection, which precludes collection for a full 60 second run time. Therefore, there are not instantaneous updates to the beam profile; the BeamGage collects for no more than 10 seconds at one time, whereas the Hamamatsu camera and power meter collect data for a full 60 second interval.
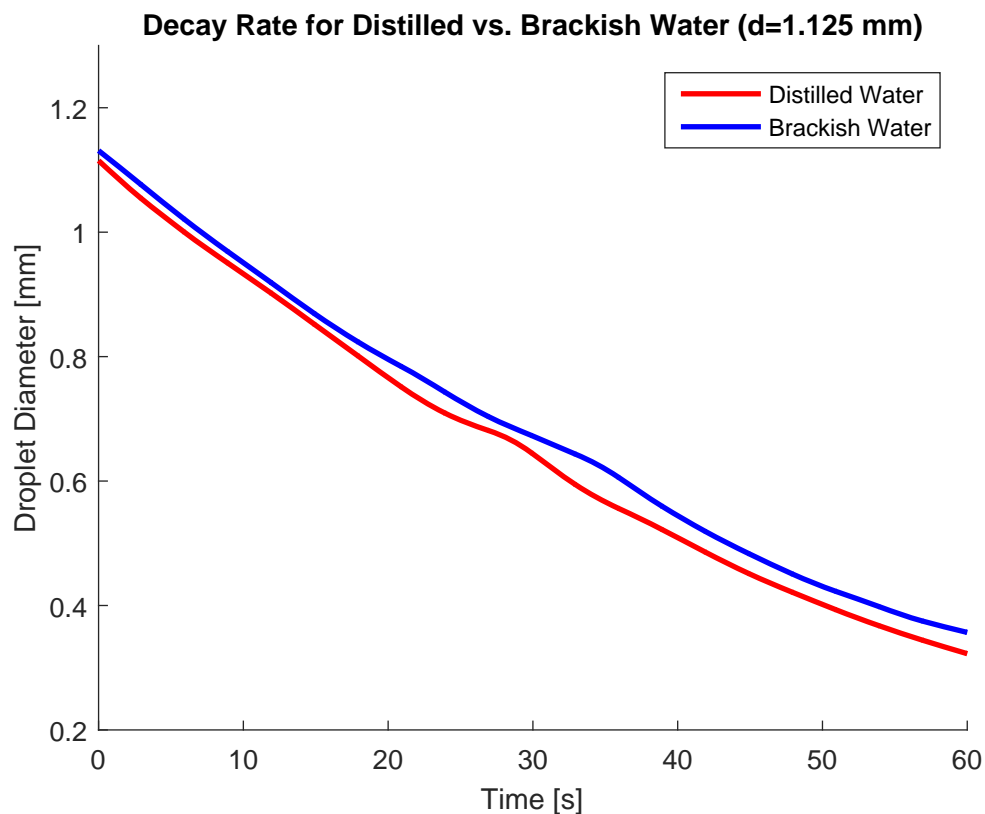
Coupling for Droplet D=1.125 mm

Figure 18: Decay Rate for 1.125mm Drop

The first observation upon looking at the race of decay for the droplet is the lack of latent heating. The loss of mass by the droplet, as evidenced by the decreasing diameter registered by the camera, shows that there is immediate mass loss when the HEL is turned on. This is likely due to local heating that overcomes the induced convection within the droplet. Video analysis shows mixing occurs within the droplet, slowly at the outset and then with increasingly rapid pace. However, in the initial vaporization, mixing is minimal. This means that the droplet face that is being irradiated experiences intense heating, and vaporization begins through nucleate boiling almost instantaneously. The viscosity of the fluid prevents mixing, and local vaporization begins before the entire droplet reaches the critical temperature for boiling to occur. This phenomenon takes place for both distilled and turbid water samples.

In the smaller droplet ranges, the decay rate for distilled and turbid water is very similar. The apparatus used to measure absorptivity of the water samples has an experimental photometric accuracy greater than the measured difference between the two samples. The distilled water sample has an absorptivity coefficient of approximately 1.48%. In comparison, the measurements for the turbid sample varied from 1.2% to 1.7%; in further experiments, it will be necessary to devise a more rigorous method for determining this absorptivity. However, the turbid sample is known to have particulate matter as well as concentrations of a variety of ions. The focus here is on the behavior of the droplet when comparing a pure sample to an impure sample. In practice, an operational HEL will experience contact with water varying in salinity and turbidity, and therefore the comparison is useful in seeing whether or not a significant effect results from an impure sample. At the 1.125mm drop size, the effect is insignificant, but it appears that the brackish water sample decays slightly slower. This change is within the error caused by jitter, but larger droplet sizes show more pronounced effect.
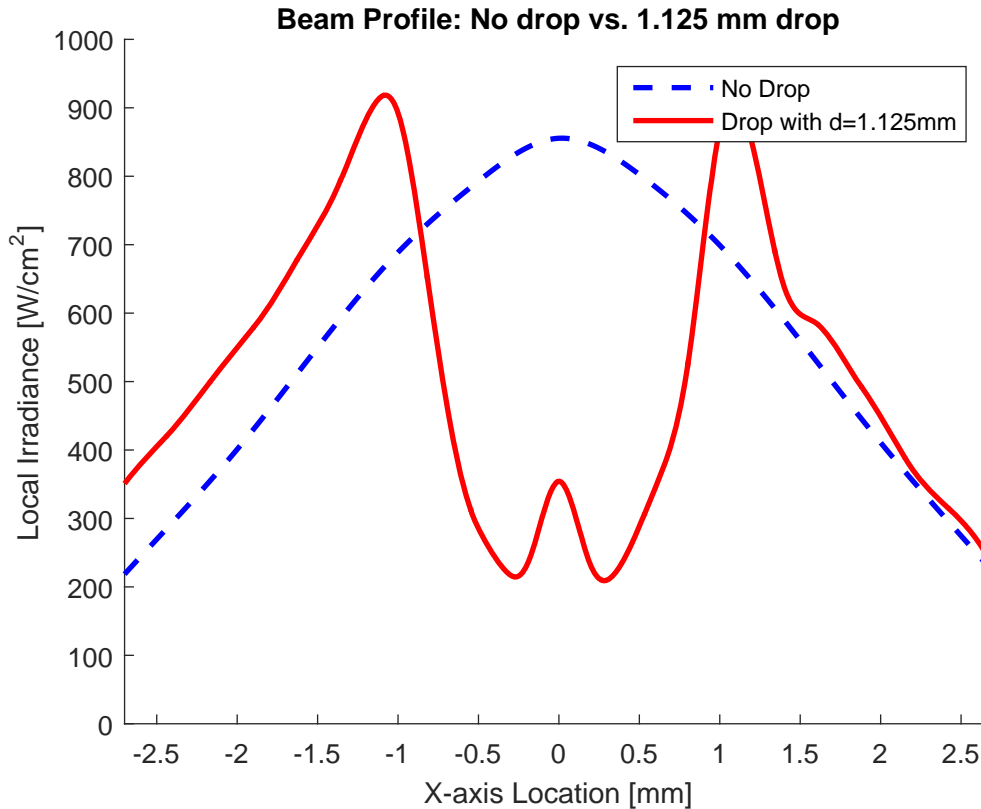
Figure 19: Beam Profile Comparison 1.125mm Drop

In the absence of a drop, the beam profile is evenly distributed. After interacting with the droplet, the beam loses power and has reduced local irradiance in the area that passes through the drop. The overall reduction in beam power is 6.3 W due to the presence of the droplet, but the local drop in irradiance by the part of the beam passing through the drop is of the most consequence.

In the region 0.5mm to either side of the beam center, the beam experiences attenuation due to the drop. The greatest reduction occurs 0.3mm to either side, with a reduction of local irradiance of 73.9%. This does not account for the spike in irradiance around the beam's centroid. This apparent increase in energy is due to diffraction around the droplet rather than a focused concentration of energy. The diffraction phenomenon causes peaks to either side in the affected beam profile as well. The droplet has a spreading effect upon the beam, causing the BeamGage to register apparent increases in irradiance. The same effect is seen in the right and left peaks that appear to register intensities of approximately 100W/cm^2 greater than the peak intensity with no drop present.
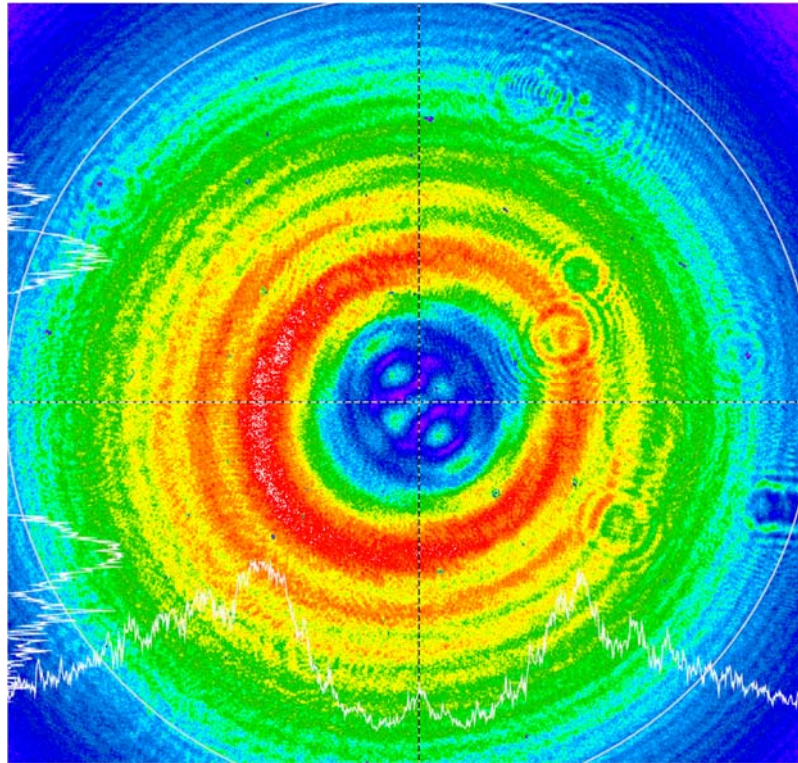
Figure 20: BeamGage image of 1.125 mm drop during HEL strike

There are several observations of importance when viewing the BeamGage results. In addition to the numerical data that allows for finding the power distribution across the beam's cross-section, inspection gives us several meaningful results.

First, the drop lies very close to the centerline of the beam path, but as shown from the spike in intensity on the left side (white amongst red), the drop is slightly off-center. Care was taken to align the drop and beam using the non-HEL guide beam. However, a different set of ND filters must be used to accomplish alignment, and upon switching the filters for the HEL the apparatus is disturbed very slightly. This disturbance is enough to affect the alignment, and the result is the slightly off-center image seen above.

Secondly, the effects of diffraction are seen in two places. The light blue concentrations in the center of the image (at the drop location) are the result of diffraction around the drop. Likewise, the ridges extending radially outwards from the center of the drop to the periphery are likely the result of diffraction caused by the drop.

Due to the alignment process, the geometric top pole of the droplet points to the bottom-right corner of the image. The light blue surrounding the droplet location matches the shape of the droplet, as the image shows an oblate spheroid with major axis running from the bottom left to the top right.
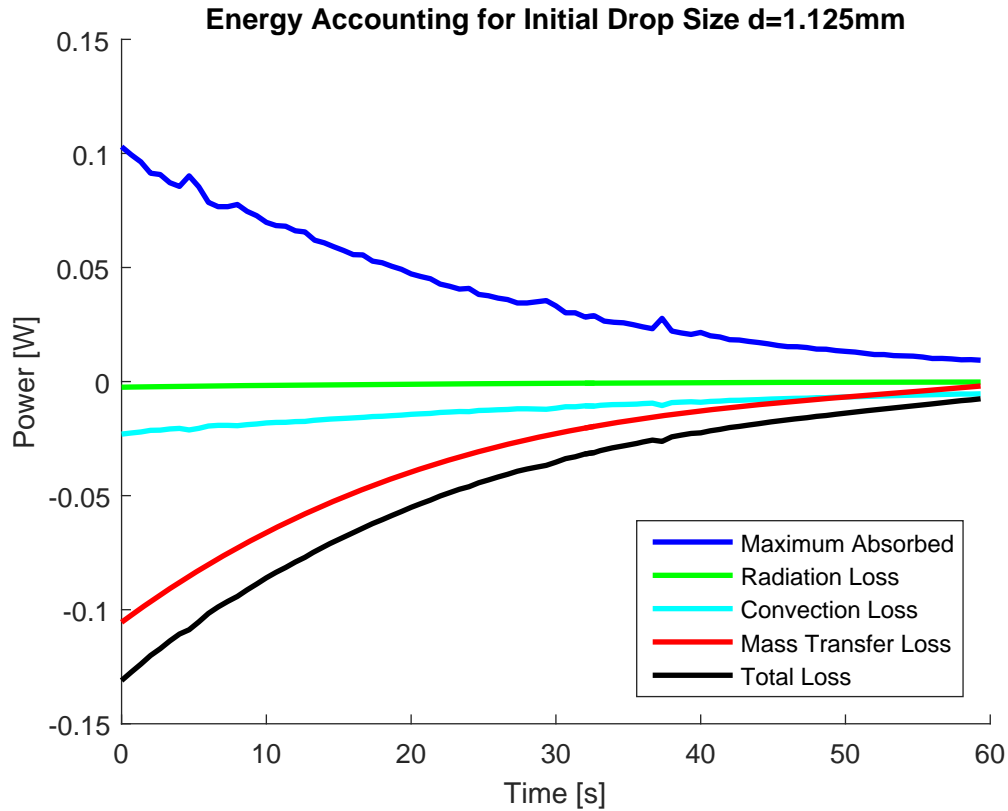
Figure 21: Energy Accounting 1.125mm

The maximum power absorbed by the droplet is a function of the droplet size and the absorptivity of the sample. Using the BeamGage in conjunction with the power meter, a value of the maximum power that the droplet can absorb is determined. This value, the blue line in Fig. 21, comes from the product of the attenuated power and the water absorptivity. This value is compared to estimates of energy loss through radiation and convection (both calculated assuming a uniform temperature distribution) and the energy required to produce the measured rate of phase change. As the irradiation of the droplet progresses, the assumption of uniform drop temperature becomes more valid. In the early stages of the interaction, the heating results in local hot spots in which nucleate boiling takes place. Therefore, the loss estimates in the early stages of vaporization are maximum estimates. As the droplet decreases in size, less energy is deposited and the rate of energy dissipation is lessened because more of the beam passes unimpeded.

Table 8: Summary of Results for Initial Diameter d=1.125mm

Measurement	Value	Units
Total Initial Power	107	W
Total Power after interaction	100.7	W
Total Reduction in Power	-6.3	W
Maximum Local Irradiance Reduction	73.9	%
Initial dV/dt	-0.0488	mm^3/s
Final dV/dt	-0.000904	mm^3/s

The two values most indicative of the droplet's effect upon the beam are the local irradiance reduction and the rates of volume change. A larger droplet has both greater volume and more surface area, resulting in more energy deposited, as well as more opportunity for energy dissipation. This is due to the dependence of each attenuation mode upon the size of the drop. Local irradiance reduction occurs at the point in the beam that passes directly through the droplet, and emphasizes the droplets ability to affect the intensity of the HEL. The droplet begins vaporization quickly, but the majority of the beam interacting with the drop is attenuated.

Coupling for Droplet D=1.25mm

The maximum power absorbed by the droplet is a function of the droplet size and the absorptivity of the sample. Using the BeamGage in conjunction with the power meter, a value of the maximum power that the droplet can absorb is determined. This value, the blue line in Fig. (), comes from the product of the attenuated power and the water absorptivity. This value is compared to estimates of energy loss through radiation and convection (both calculated assuming a uniform temperature distribution) and the energy required to produce the measured rate of phase change. As the irradiation of the droplet progresses, the assumption of uniform drop temperature becomes more valid. In the early stages of the interaction, the heating results in local hot spots in which nucleate boiling takes place. Therefore, the loss estimates in the early stages of vaporization are maximum estimates. As the droplet decreases in size, less energy is deposited and the rate of energy dissipation is lessened because more of the beam passes unimpeded.
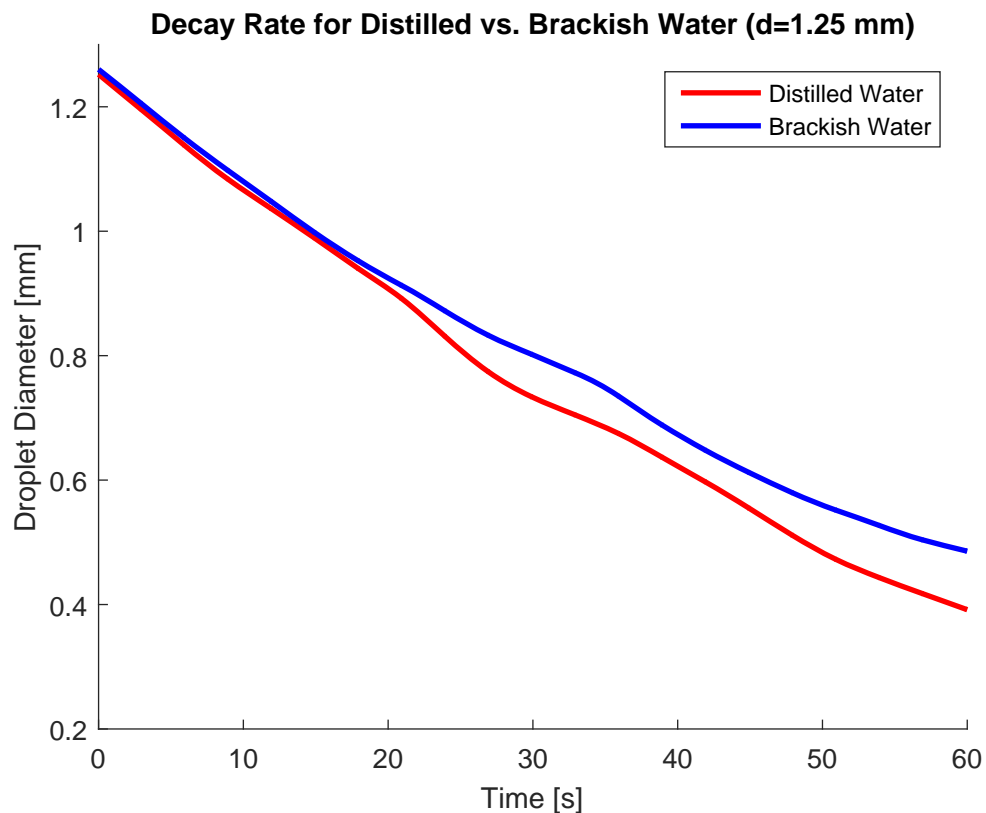

Figure 22: Decay Rate for 1.25mm Drop

In a droplet of slightly larger initial diameter, the effect of the turbid water sample is more pronounced. Both water samples display the lack of a sensible heating period seen previously. In this series of tests, the final drop sizes show more separation, as the distilled water displays a larger decay rate towards the end of the vaporization.
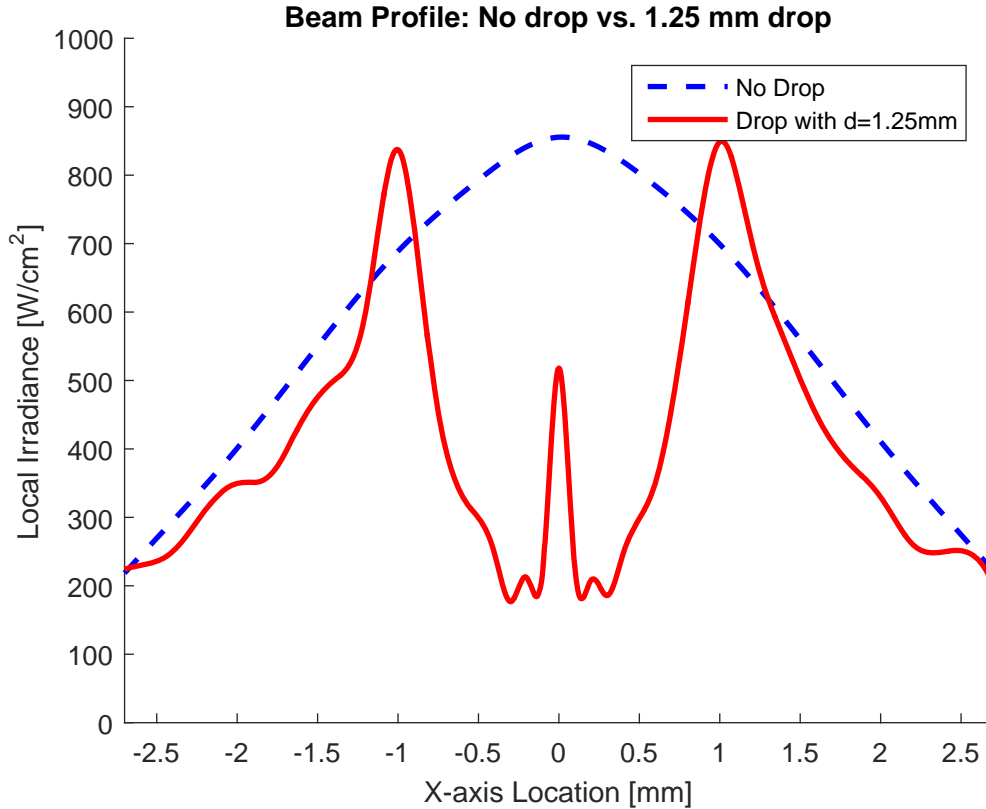

Figure 23: Beam Profile Comparison 1.25mm Drop

The decrease in HEL power in the presence of a 1.25mm drop is greater, as total power attenuation is 8.5 W. Diffraction effects are slightly more pronounced in the 1.25mm runs, with secondary peaks occurring around the beam centroid. It is unclear why the secondary peaks occur +/-0.25mm from the centroid. This is likely due to noise within the BeamGage results rather than a concentration of power or meaningful result.

The local irradiance is reduced further as well; the reduction in irradiance at the point of most interference from the drop is 78.5%. This establishes a positive relationship between drop size and power reduction in the HEL; a modest increase in drop size leads to less of the affected part of the beam reaching the power meter.
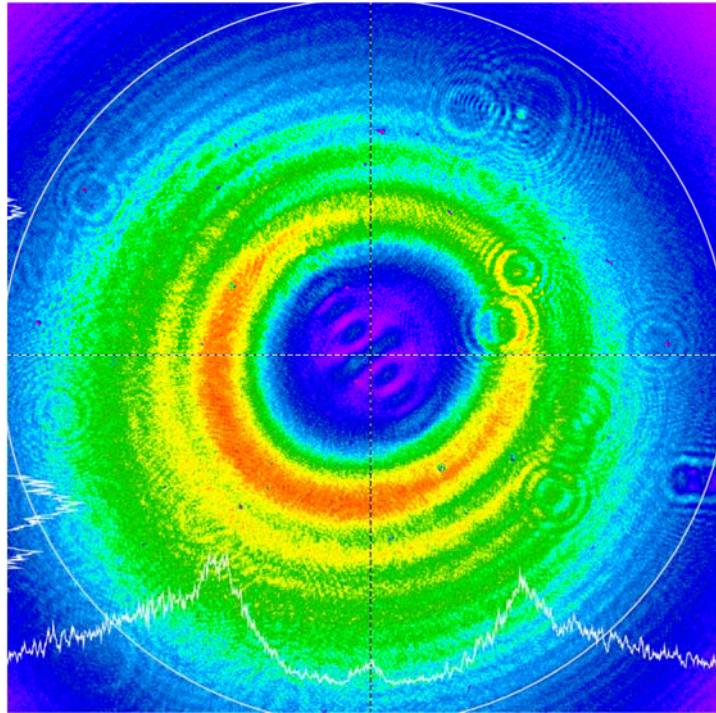
Figure 24: BeamGage Image of 1.25 mm Drop During HEL Strike

The image in Figure 24 shows the BeamGage result for a laser strike on a 1.25mm drop. Diffraction is still a powerful force in determining the character of the energy distribution, with secondary power peaks occurring in the center of the drop as well in the periphery. This droplet was slightly more oblate, resulting in the peaks centered on the crosshairs that form one large peak running from the bottom left to the top right, rather than two distinct peaks.
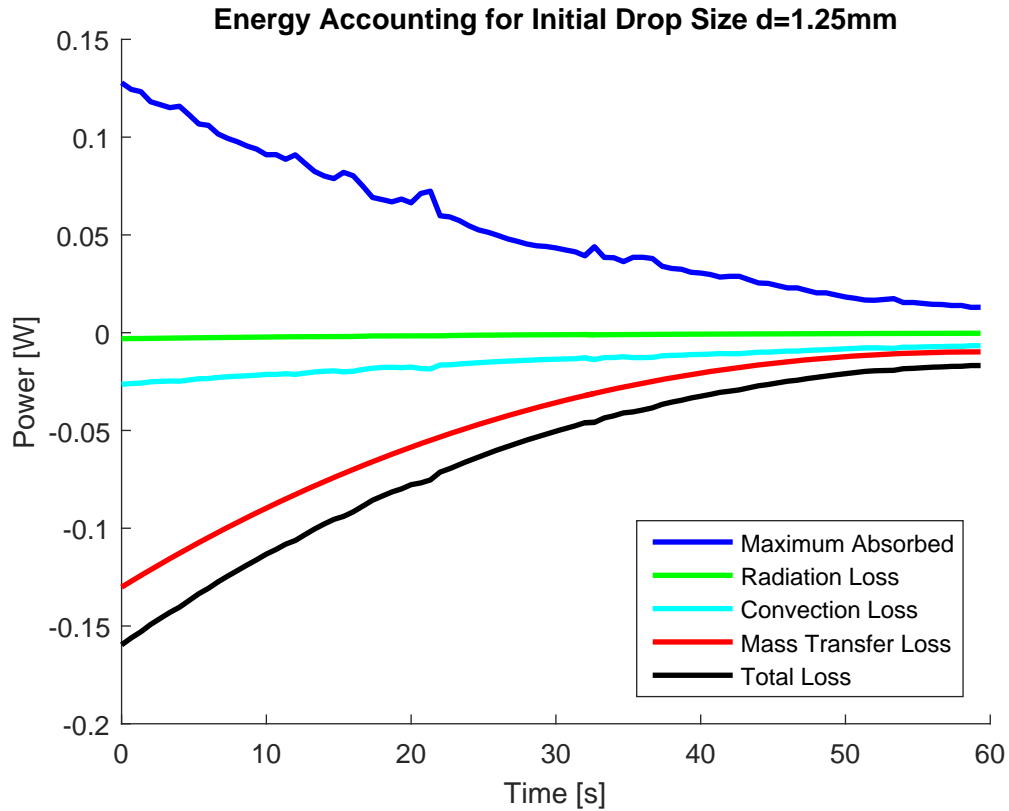
Figure 25: Energy Accounting 1.25mm

As the droplet size increases, the power received by the droplet increases as well. The maximum absorbed value refers to the best case scenario for absorption, in which all of the energy that may be absorbed is in fact absorbed into the water droplet. As with the 1.125mm drop, the estimates for convection and mass transfer loss are generous due to the unmixed nature of the drop. Radiation exchange continues to have negligible effect on the transfer of energy between the droplet and the surroundings.

Table 9: Summary of Results for Initial Diameter d=1.25mm

Measurement	Value	Units
Total Initial Power	107	W
Total Power after interaction	98.5	W
Total Reduction in Power	-8.5	W
Maximum Local Irradiance Reduction	78.5	%
Initial dV/dt	-0.0603	mm^3/s
Final dV/dt	-0.00454	mm^3/s

A larger droplet size results in larger decay rates for the drop both at the outset of the irradiation and upon completion of the run. Local reduction in power also increases, and the total power attenuated throughout the interaction indicates that the beam is not refocused, and is instead scattered by diffraction.
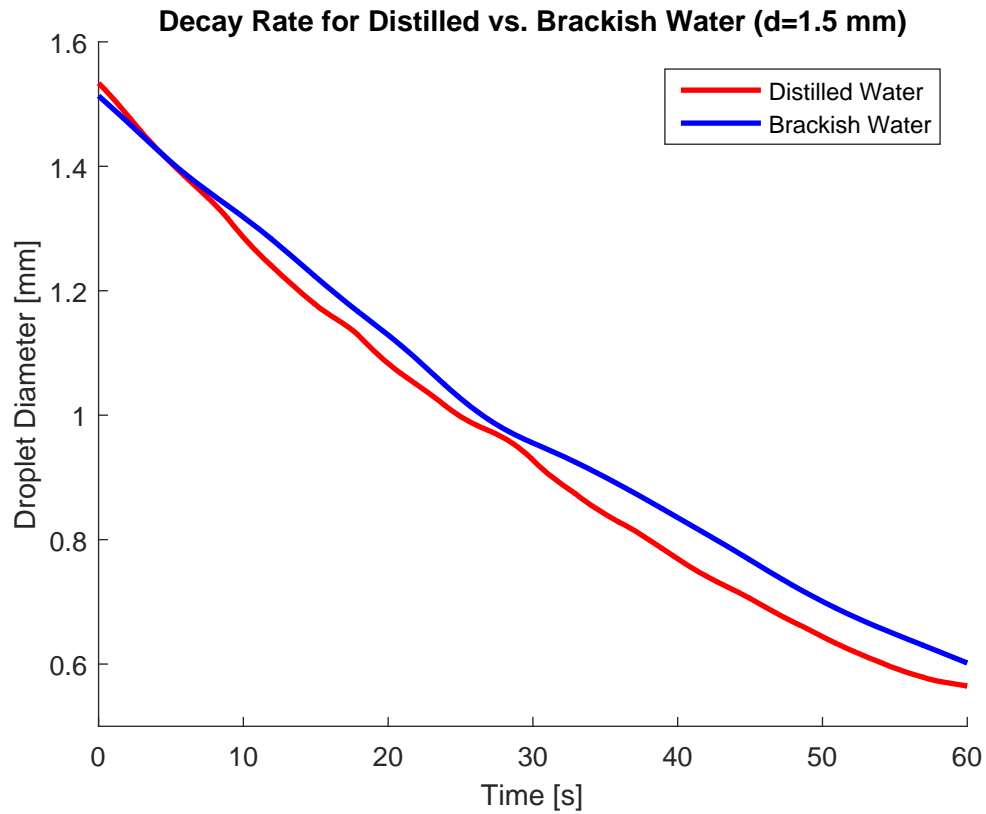
Coupling for Droplet D=1.5mm

Figure 26: Decay Rate for 1.5mm Drop

For an initial drop size of 1.5mm, a similar difference in final drop size is achieved compared to the results for the 1.25mm drop. Of note, the initial size of the distilled drop is slightly larger than that of the turbid drop. The differences between decay rates of the distilled and turbid samples are within the range of error that could be produced by the experimental method (image analysis). However, there is a clear trend that the distilled water samples decay at a faster rate than the brackish samples.
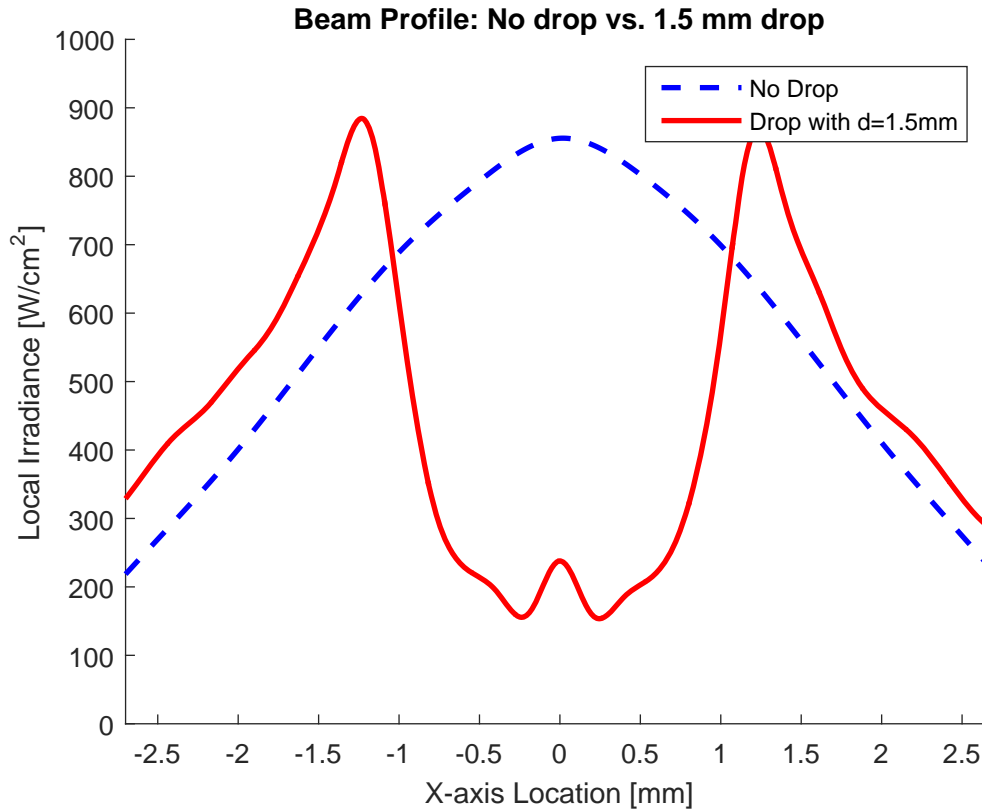
Figure 27: Beam Profile Comparison 1.5mm Drop

The trend in decreased local irradiance continues with the 1.5mm drop. Accounting for the effects of diffraction, the decrease in local irradiance is 81.2%. There was much less noise in the BeamGage results for the 1.5mm drop when compared to the 1.25mm drop. By inspection, the effects of diffraction in the drop's geometric shadow zone are lessened, but of the same magnitude to the outside of the drop when compared to previous results.
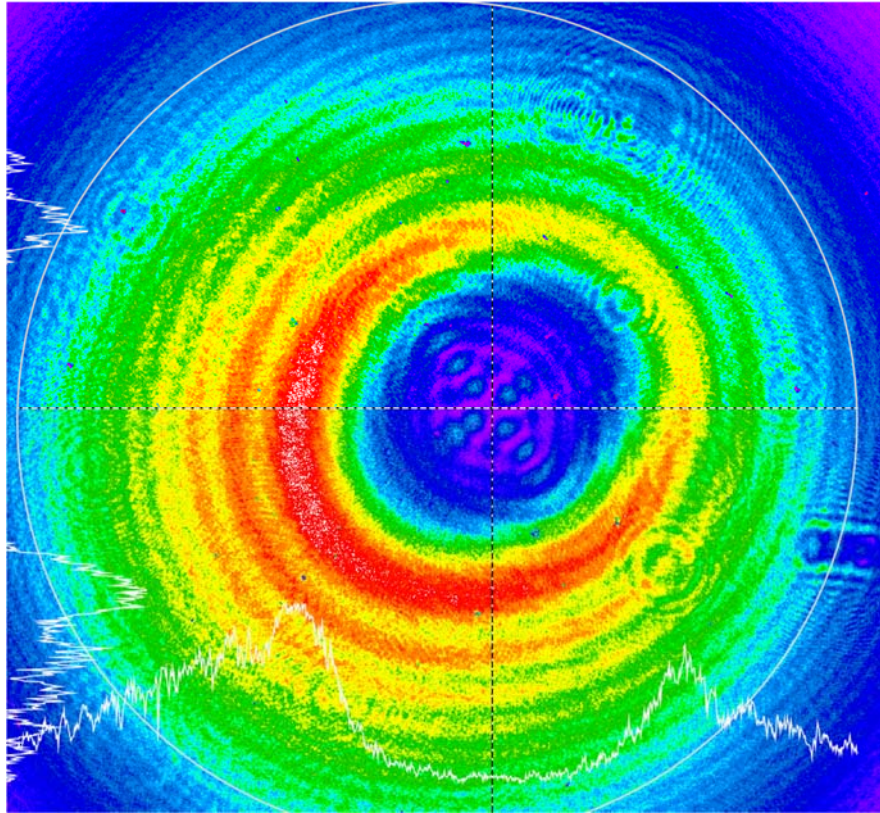
Figure 28: BeamGage Image of 1.5 mm Drop During HEL Strike

The 1.5mm drop was the most poorly centered of the presented results. The same diffraction effects are seen both in the droplet area as well as in the periphery surrounding the drop.
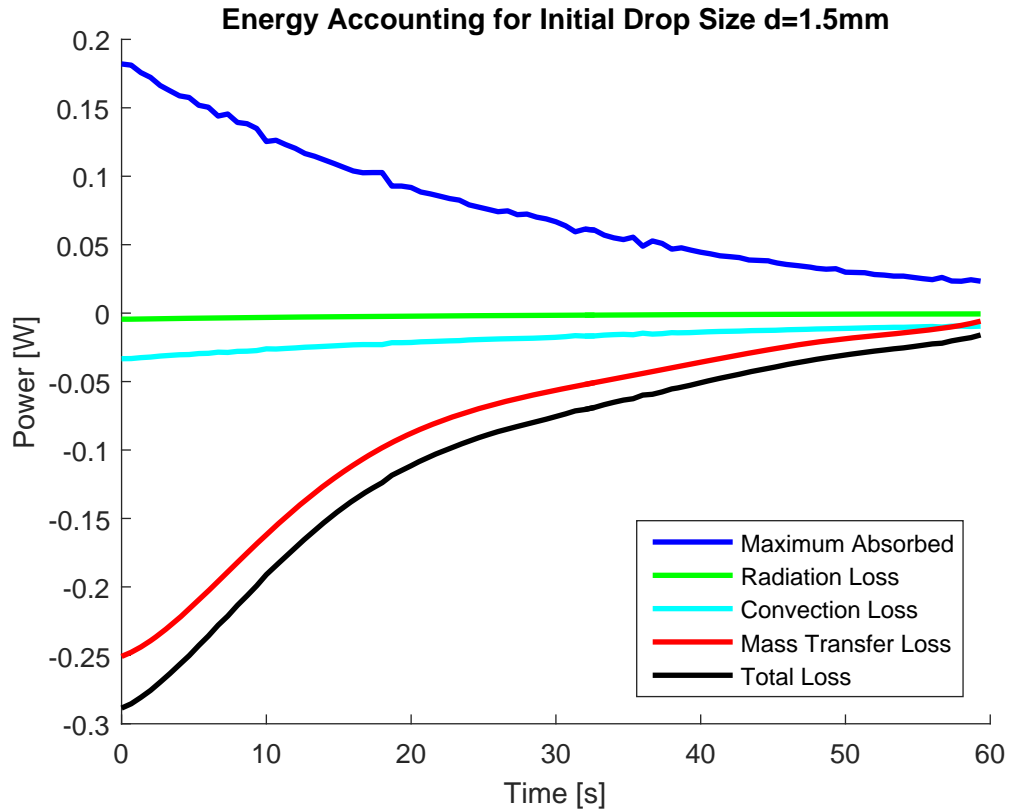
Figure 29: Energy Accounting 1.5mm Drop

As the size of the drop increases, the discrepancy between maximum absorbed energy and total theoretical loss increases. Local vaporization continues to be the primary mode of mass transfer, and convection dissipates a significant amount of energy. However, both of these approximations rely on the thorough mixing of the drop to establish a uniform temperature profile. This assumption is not valid, and as the droplet size increases, the droplet will take longer to become thoroughly mixed.

Table 10: Summary of Results for Initial Diameter d=1.5mm

Measurement	Value	Units
Total Initial Power	107	W
Total Power after interaction	95.1	W
Total Reduction in Power	-11.9	W
Maximum Local Irradiance Reduction	81.2	%
Initial dV/dt	-0.1160	mm^3/s
Final dV/dt	-0.0027	mm^3/s

As expected with an increase in droplet size, the total attenuation due to the droplet is greater than seen with smaller droplet sizes. The reduction in local irradiance is larger as well, as the greatest attenuation occurs across the widest part of the drop.
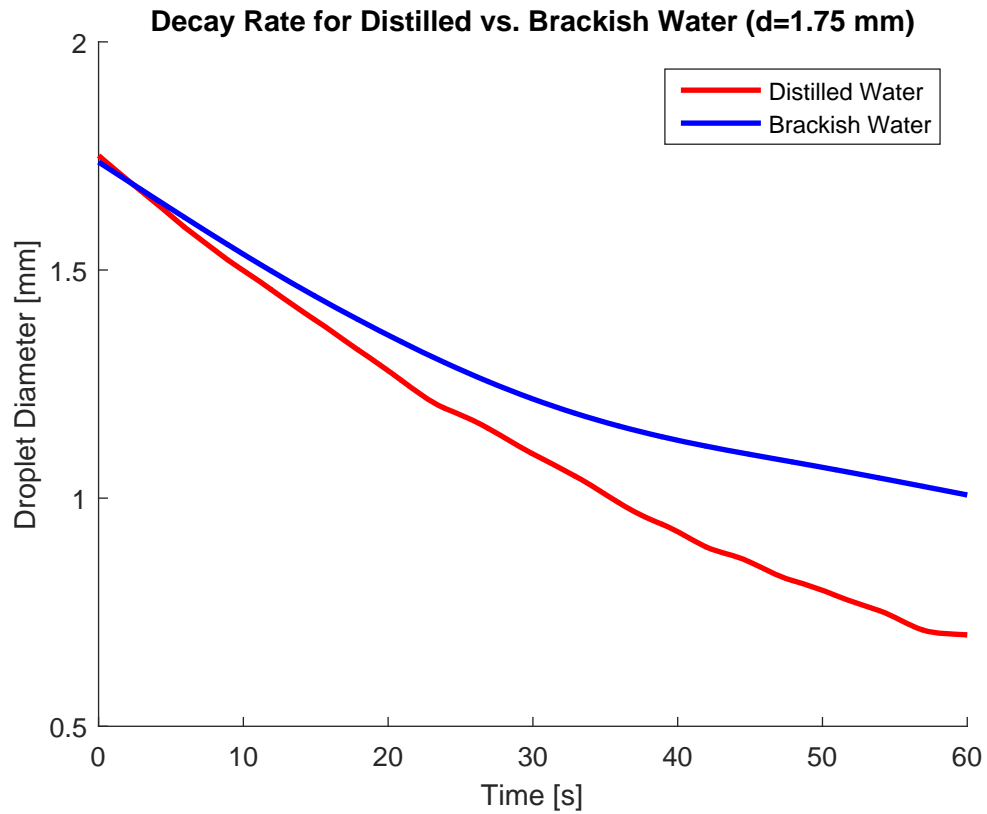
Coupling for Droplet D=1.75mm

Figure 30: Decay Rate for 1.75mm Drop

The difference between distilled and brackish sample decay rates is largest in the 1.75mm drop. As seen in Figure 30, the brackish water is much more resistant to decay as a result of the laser strike.

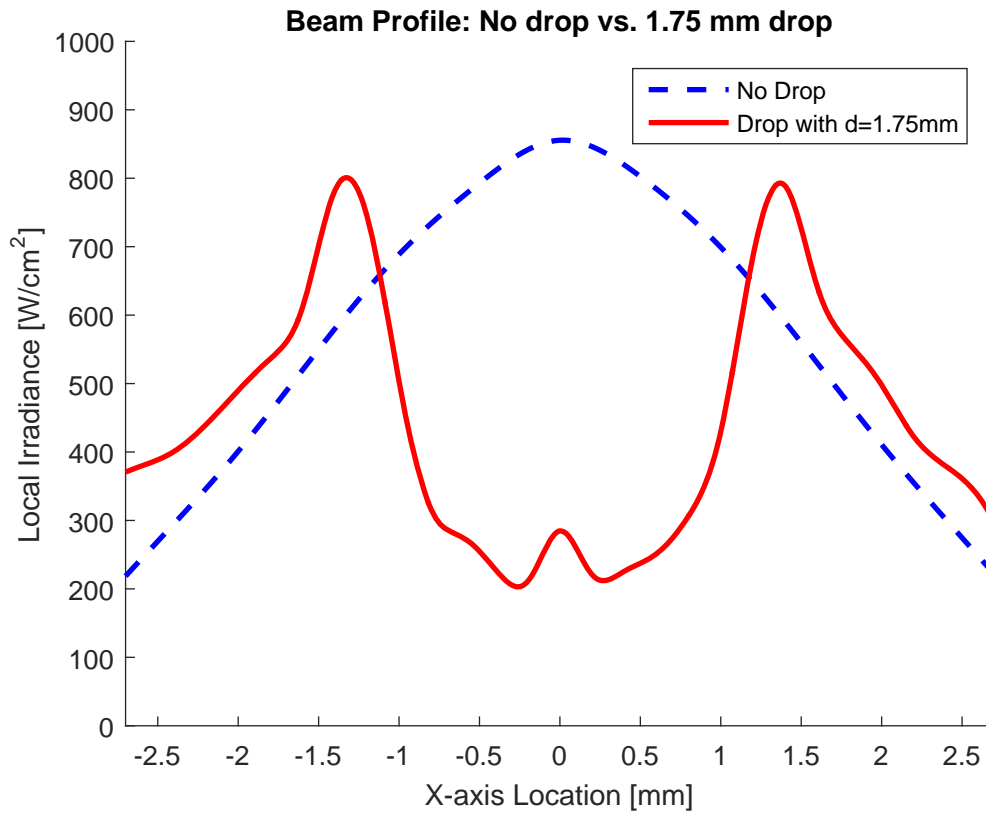Figure 31: Beam Profile Comparison 1.75mm Drop

The results from the 1.75mm run confirm that noise was likely the cause of secondary peaks in the 1.25mm drop run. Figure 31 shows the characteristic diffraction peaks to the left and right of the droplet location, and the smaller peak in the shadow zone behind the drop. With each successive increase in drop size, the area of energy blocked increases to match.
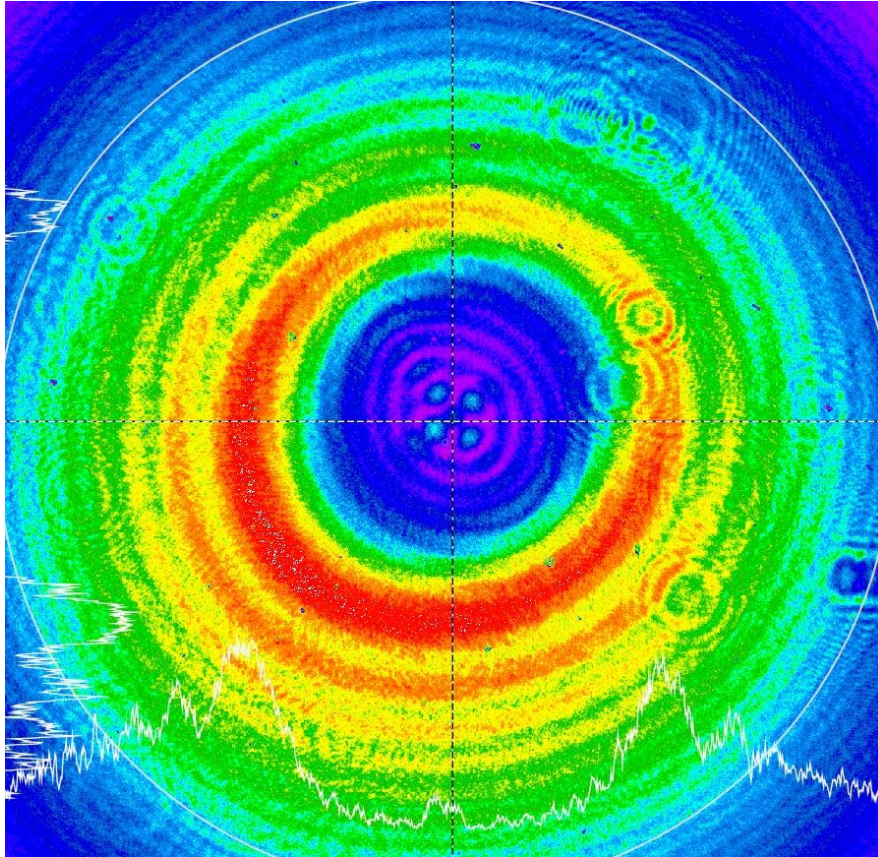
Figure 32: BeamGage Image of 1.75mm Drop During HEL Strike

The image for the 1.75mm drop irradiation is similar to the results for 1.125mm and 1.25mm. While the shadow zone behind the droplet contains the characteristic blue dots found in the previous runs, it also begins to display the rings of variable intensity that are shown throughout the rest of the image. This confirms that diffraction is in fact responsible for the HEL's propagation around the drop.

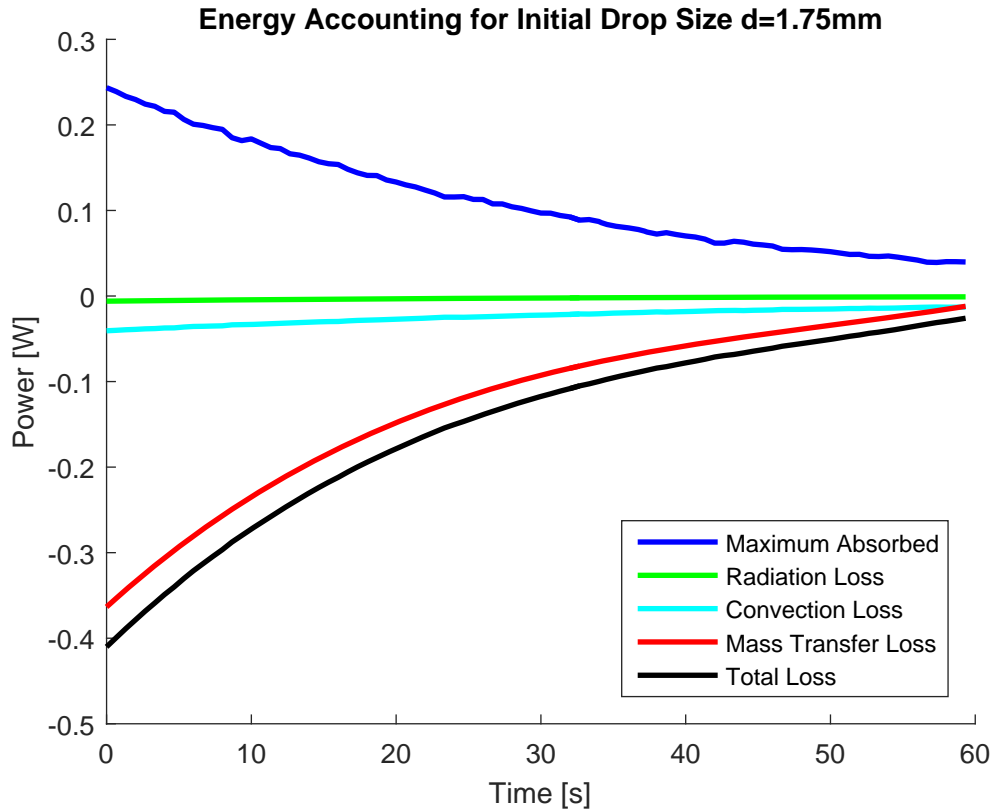**Energy Accounting for Initial Drop Size d=1.75mm**

Figure 33: Energy Accounting 1.75mm Drop

With each subsequent increase in droplet size, the discrepancy between the maximum absorbed energy and total theoretical loss grows. The total loss increases at a greater rate as it is dependent on volume of the droplet, rather than area. The increase in volume also leads to a longer time necessary to heat the entire droplet to the boiling temperature.

Table 11: Summary of Results for Initial Diameter d=1.75mm

Measurement	Value	Units
Total Initial Power	107	W
Total Power after interaction	92.8	W
Total Reduction in Power	-14.2	W
Maximum Local Irradiance Reduction	76.09	%
Initial dV/dt	-0.1681	mm^3/s
Final dV/dt	-0.0055	mm^3/s

The trends seen in the previous three droplet sizes are repeated here. Local irradiance is slightly larger than in the 1.5mm run, although not by much. Decay rate continues to grow larger with the increased size of the drop. The reduction in local irradiation does not continue to grow, but remains in the same range as previous values.
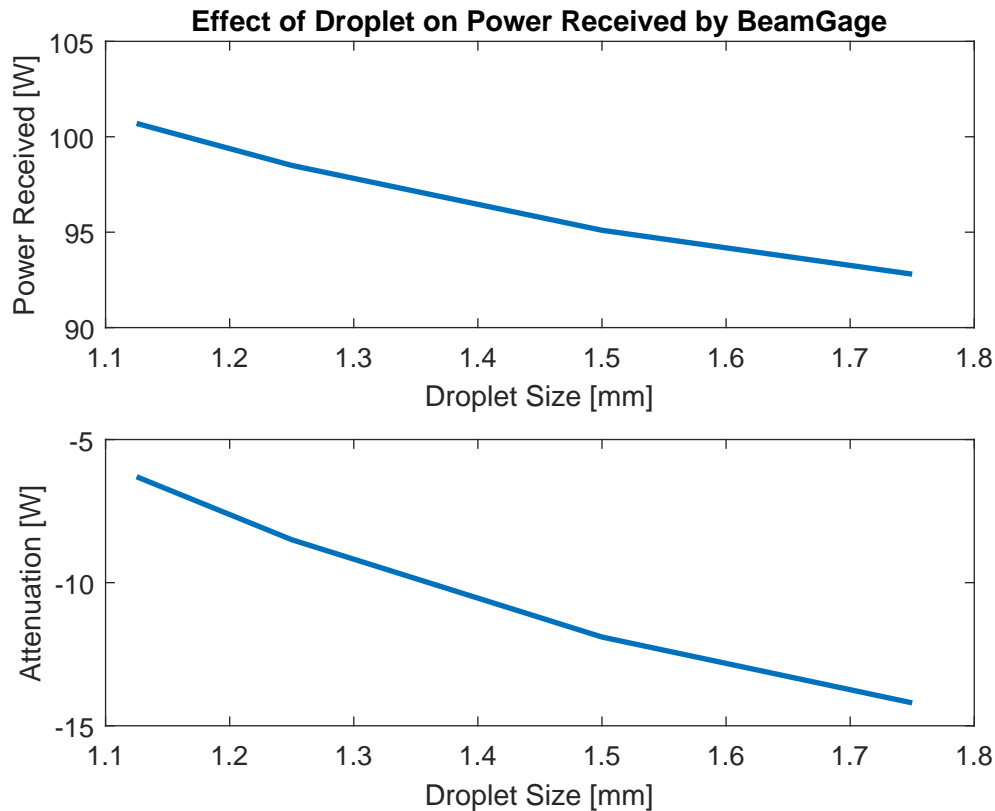
Figure 34: Effects of droplet on power received

For a power setting of 100 W, the HEL is consistent in producing 107 W. The top figure shows the power that is registered by the power meter after the HEL interacts with the droplet. A linear relationship develops between the power received and the size of the droplet; as the drop size increases, less power reaches the power meter. The power meter collects energy across a wider area than the beam profiler, and it significantly larger than the drop. Therefore, the power cannot be assumed to be focused in the same 5mm diameter aperture that the HEL produces. Though very little power is absorbed by the drop, as shown in previous BeamGage results, the overall attenuation is significant. For a 1.75mm drop, over 10% of the power produced by the HEL does not reach the power meter.

The level of attenuation is significantly larger than the contribution from heat transfer mechanisms. From the 1.75mm drop analysis, less than 0.5W is lost to the combination of mass transfer, convection and radiation. Therefore, the majority of power attenuation is due to scattering when the droplet strikes the drop, and again as it exits. Most reflection presumably occurs from the front and rear faces of the drop, but reflection was not measured independently in these experiments.
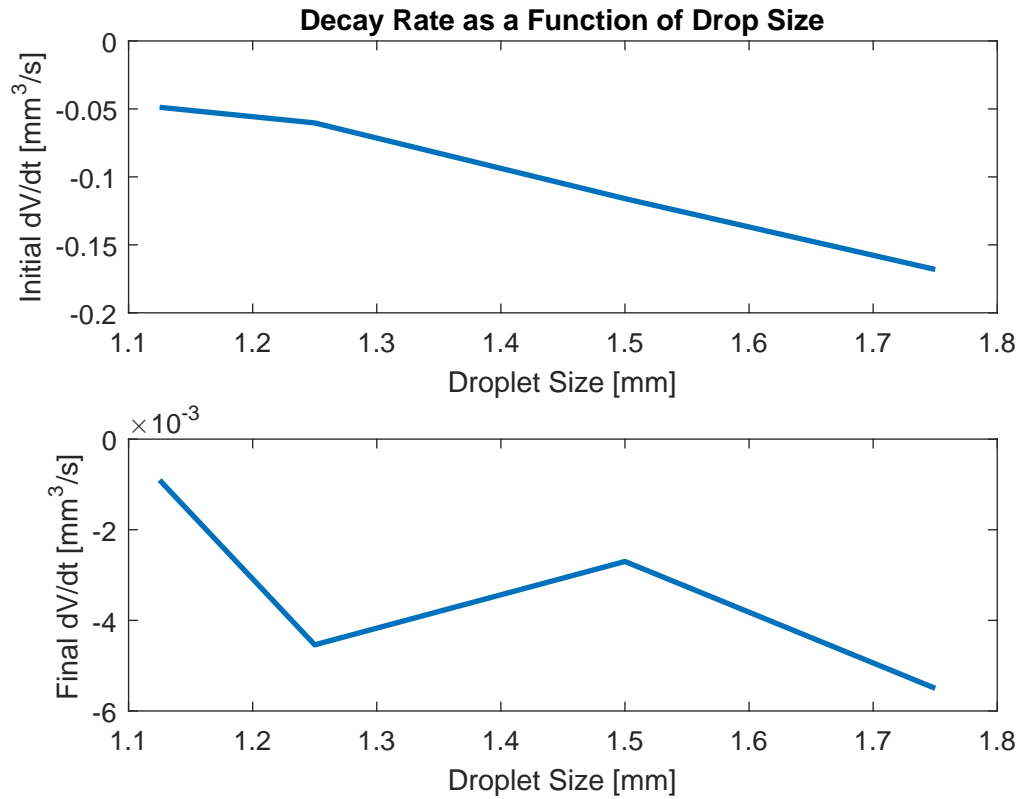
Figure 35: Decay Rate as a Function of the Initial Drop Size

Table 12: Decay Rate across Drop Diameters

	1.75mm	1.5mm	1.25mm	1.125mm
Initial Decay Rate [mm^3/s]	-0.1681	-0.1160	-0.0603	-0.0488
Final Decay Rate [mm^3/s]	-0.0055	-0.0027	-0.00454	-0.000904

Shown above are the decay rates at the onset of the irradiation event (top), and at the end of irradiation. By inspection of the top graph, decay rate correlates well to the drop size in the same way as attenuation of power. The larger the drop size, the faster the drop will decay. The trend at the end of irradiation is less evident, though this is likely a function of the small decay rate, which is an order of magnitude less than the initial rate. The behavior of the drop at the end of irradiation, when it is smallest, confirms that larger drop size lends itself to quicker decay. The smaller the droplet size, the slower the drop will decay. This makes sense because the reduced area presents a smaller interface between the drop and HEL, and the path length through the drop is reduced, so less energy is deposited which slows the rate at which energy may be released through phase change.
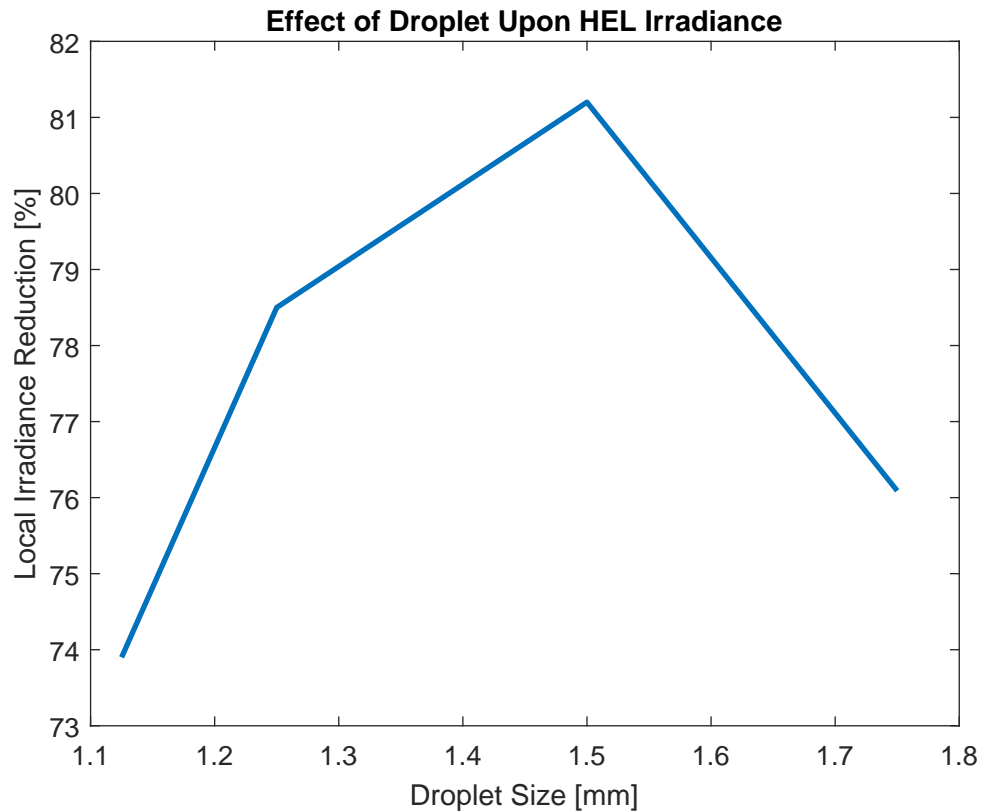
Figure 36: Effect of the Drop Size on the Local Irradiance at the Center of the Irradiated Drop

Figure 36 shows the reduction in irradiance through the center of the droplet. There is no clear trend developed in the graph, but this may be partially due to the smoothing applied to the BeamGage results. The BeamGage representation of the beam profile contains significant noise, so upon smoothing the curve the exact reduction may not be exact. However, it is clear that the drop causes significant attenuation of energy, ranging from 75-80%. As droplet size increases, the attenuation would grow larger until the amount that passed through would be dominated by the absorption coefficient of the specimen. At these size, the geometry of the droplet has an effect and scattering considerations are also significant contributors to the decrease in power that makes it all the way to the power meter. These percentages are representative of the amount blocked at the peak of the droplet's blocking ability; as seen above, the majority of energy still makes its way to the power meter despite the presence of the drop.

Coupling Analysis for Droplet Sizes 1.125mm-1.75mm
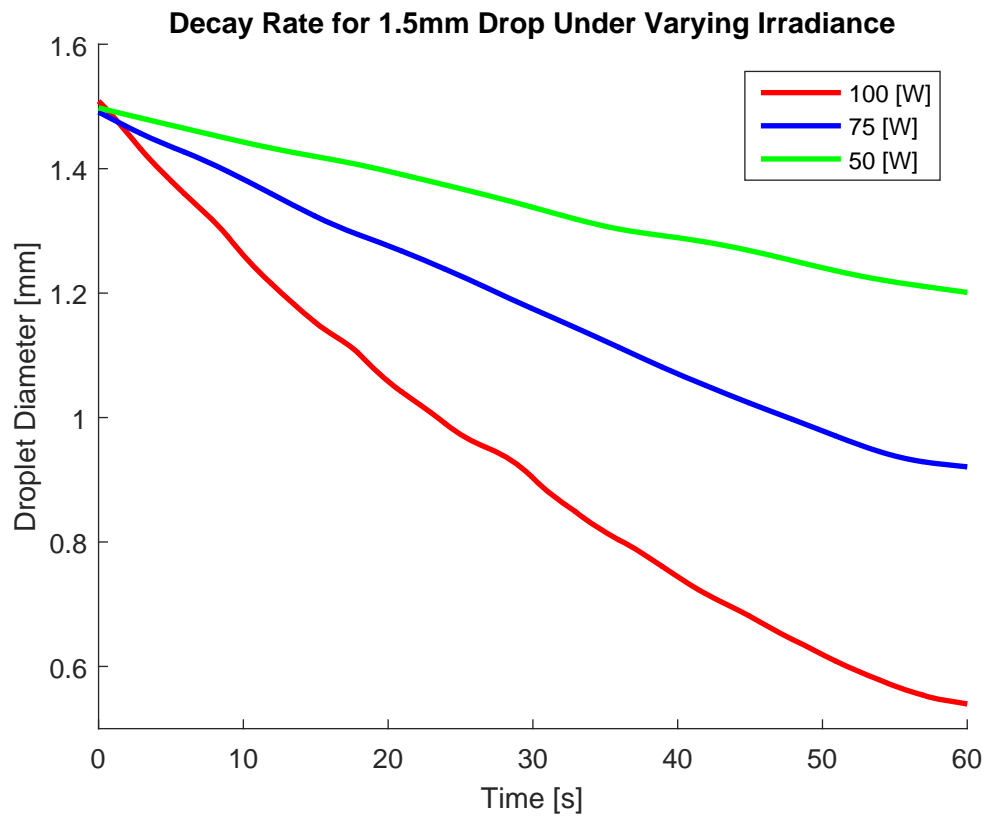
Figure 37: Decay Rate due to Various Levels of Irradiance

The above figure shows the comparison between three different power levels for the HEL interacting with a 1.5mm drop. Decay rates corresponding to each power level are shown in the table below.

Table 13: Decay Rate across operating power levels (d=1.5mm)

	100 W	75 W	50 W
Initial Decay Rate [mm³/s]	-0.1160	-0.0521	-0.0253
Final Decay Rate [mm³/s]	-0.0027	-0.0012	-0.0131

With each decrease in power of 25W, or 25% of peak operating power, the corresponding decrease in decay rate is approximately 50%. Thus, even a modest increase in power may result in a significantly increased rate of decay for the droplet.

CONCLUSIONS

These experiments were successful in exploring the coupling between a large water drop and an HEL. The development and testing of the data collection process proved the concept and allowed for observation and quantification of the interaction. Analysis of the data collected allowed for several conclusions to be drawn about the interaction, and will inform future investigation.

Data collection took place using a high-speed visible camera in conjunction with a beam profiler and power meter. The combination of these devices allowed for the characterization of the droplet and the HEL concurrently. MatLab was used for both collection of the video and beam profiles, and also for the image analysis from video frames. A separate laboratory computer contained the software necessary to run the beam profiler. The laser was run without a drop in the levitator in order to establish baseline operation, and droplets were levitated and observed on video without a laser strike in order to establish standard behavior.

From the beam characterization, it was found that the beam profile is similar to the nominal profile provided by the manufacturer. The beam profiler was subject to considerable noise, so multiple runs were used to confirm the profile of the beam without an object in its path, and then again once droplets were placed in the cross-section of the beam.

Both brackish and distilled water samples experienced decay as a result of the irradiation event, although a clear trend was established that sample type was more important as droplet size increased. Larger droplets of brackish water decayed more slowly than their distilled counterparts. A combination of visual inspection and analysis in MatLab showed that the drop heats unevenly, and it is not until the droplet has been irradiated for some time that a uniform temperature profile is achieved.

Several conclusions may be drawn from the coupling of the beam profiles with the droplet decay rates. There is a direct relationship between droplet size and rate of mass loss for a given drop size; as the drop size increases, so does the path length through the drop. This, together with greater incident power, leads to faster decay. Similarly, attenuation is larger for greater droplet sizes. The relationship between droplet size and local attenuation is relatively consistent; across all drop sizes, local attenuation varied by 5%. Diffraction may have been responsible for some discrepancies, as the results from the BeamGage showed laser profiles that had been affected by diffraction in numerous ways.

FUTURE WORK

A future Trident project will be focused on determining the exact heating regime for the droplet through the irradiation process. Infrared camera use will assist in providing a more exact estimate of surface temperature and provide a better theory for the temperature gradients within the droplet. Temperature data will hopefully help explain the possibly contradictory observations of immediate phase change upon irradiation (suggesting local regions of high heat rate) and vigorous mixing inside the drop (which would break up pockets of high temperature fluid.) The existing apparatus can be used to continue experimentation with minor changes.

Other steps in the process will be to develop a model that can account for transient effects of laser propagation and phase change, and eventually to apply these findings to a field of droplets, as would be encountered in the operational use of an HEL.

REFERENCES

[1]= O'Rourke, R. (2014, April 1), "Navy Shipboard Lasers for Surface, Air, And Missile Defense: Background and Issues for Congress," Congressional Research Service.

[2]= "China Develops Laser System Against Drones," Yahoo.com (2014, November 4).

[3]= "Counter Directed Energy Weapons," (n.d.). Retrieved November 26, 2014, from http://www.onr.navy.mil/en/Media-Center/Fact-Sheets/Counter-Directed-Energy-Weapons.aspx

[4]= Mobley, C. (1994). *Optical Properties of Water*. In M. Bass (Ed.), *Handbook of Optics* (2nd ed.). McGraw Hill, New York, NY.

[5]= Moran, M.J., Shapiro, H.N., Boettner D.D. and Bailey, M.B. 2011, *Fundamentals of Engineering Thermodynamics,* 7th ed., John Wiley & Sons, Inc., Hoboken, NJ.

[6]= Nielson, P.E., 1994, *Effects of Directed Energy Weapons*, Library of Congress, Washington, D.C.

[7] Armstrong, R.L and Park, B.S., "Laser Droplet Heating: Fast and Slow Regimes," Applied Optics 28 (17) 1989

[8]= "Basics About Ultrasonic Levitation". (2014). In *Ultrasonic Levitator Manual*. Germany: Tec5- Technology for Spectroscopy.

[9]= Saha, A., Basu, S., and Kumar, R., "Particle image velocimetry and infrared thermography in a levitated droplet with nanosilica suspensions." Exp Fluids Vol 52, 2012.

[10]= Dash, S., Chandramohan, A., Weibel, J., and Garimella, S., "Visualization of buoyant convection in droplets on superhydrophobic surfaces." 67th APS DFD Meeting, San Francisco, CA, November 2014.

[11] IPG Photonics YLR-100-AC Instruction Manual. Publication P21-010067, Rev. B, 2009.

[12] C. Lloyd, Ablative Polymeric Materials for Near-Infrared High-Energy Laser Beam Diagnostics, Journal of Directed Energy, 3, 2009.

[13] T. Bergman, Introduction to Heat Transfer, Wiley Publishing, Jefferson City. 2011.

[14] L. Kou and D. Labrie and P. Chylek, "Refractive indices of water and ice in the 0.65-2.5um spectral range," Appl. Opt., 32, 3531--3540, (1993).

APPENDIX A: LASER SPECIFICATION

An IPG Phototonics model YLR-100 AC High Energy Laser (HEL) was used in the experiments. The laser is run from a console in the laser lab through a GUI on Matlab.

Figure 1A: Laser Generation Unit

The laser is produced the rack mounted unit shown above. The lazing media is contained in a coaxial fiber optic cable. This allows for highly efficient transfer from the pumping diode. The output is another fiber optic cable that leads to a beam collimator that produces the final 5.0mm $1/e2$ beam diameter. The fiber is made of Ytterbium doped Yttrium Aluminum Garnet (Yb:YAG).

Figure 2A: Beam Collimator

IPG YLR-100 AC HEL	
Output	Continuous Wave (cw)
Maximum Nominal Power	100 W
M^2	1.07 (max 1.1)
$1/e^2$ Beam Diameter	4.5-5.5mm
$1/e^2$ Beam Divergence	0.3 mrad
Cooling	Forced Convection
Power Consumption	400 W
Wavelength	Operated at 1070nm (Range 1060-1100nm)
On/Off Switching Time	30 µs

The GUI from which the laser is run has various inputs that may be changed from run to run. Beam power and time of laser shot may be adjusted based upon operating needs. Run characteristics may be saved for repeatability.

There is an interlock mechanism linked to the laser GUI that ensures that all safety features are in place before the laser may be turned on. To help with aligning measurement devices, the laser console also contains a non-destructive guide beam.

APPENDIX B: LEVITATOR SPECIFICATION

The levitator has the most degrees of freedom of any of the instruments used throughout the experiment. The apparatus is mounted on a based that has micrometer adjustment in a horizontal direction perpendicular to the beam path, as well as vertical adjustment. The base adjustment is completed first, allowed for a general alignment that will only have to be fine-tuned once a droplet has been placed in the levitator.
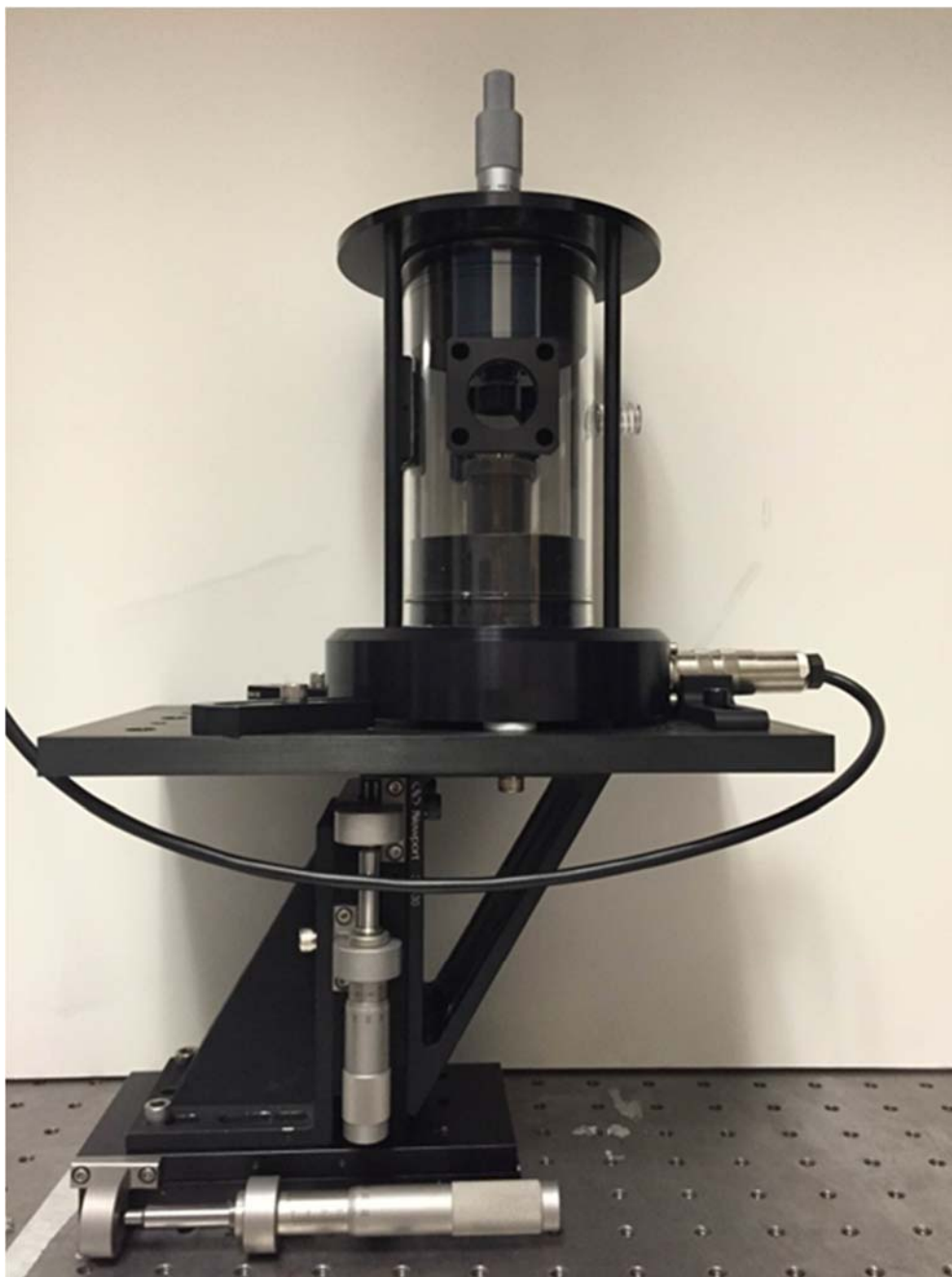

Figure 1B: tec5 Ultrasonic Levitator

Once the droplet has been placed, the guide beam is turned on to finish the alignment process. While the HEL is near-IR and thus not in the visible spectrum, the guide beam is visible and thus useful in aligning the droplet within the levitator. In order to ensure that the droplet falls within the center of the beam cross-section, the vertical and horizontal adjustment on the levitator mounting base are used. The red spot created by the guide beam falls on the power meter behind the levitator, and the shadow cast by the droplet effectively blocks the guide beam's path. When the shadow is centered within the guide beam, the system is aligned and ready for irradiation by the HEL.

Table 1B: Levitator Operation:

	Minimum	Maximum
Power Setting	4.6 W	5.7 W
Deflection of Reflector (measured from bottom position)	0 mm	3.5 mm

The power setting for the levitator is measure of the Radio Frequency (RF) power provided to generate the 58 kHz wave that levitates the droplet. The range that was found most acceptable for the test range of 0.5-2.5mm is given in Table 1. Greater power often resulted in corresponding droplet deformation, especially once radiation had commenced. It is therefore recommended that the transducer be adjusted to the greatest deflection possible without causing the droplet to wobble within the standing wave.

The technique for placing the droplet was refined over the course of multiple trials runs before data was collected, and during the initial data collection. Preliminary work was conducted using a syringe, which could provide a large droplet range but was inconsistent from trial to trial. Another problem that was identified was the issue of excessive air bubbles within the droplet. The aperture for the syringe was too large to provide consistent droplets, especially those of smaller size. Droplet size consistency and air trapped within droplet samples were resolved through a combination of technology and technique improvements. Best results were achieved when using a FisherBrand variable volume micropipette, which has a functional range of 0.5 uL to 10 uL. Research thus far has been centered on the 1.0 uL to 3.0 uL range, as the large droplet regime is centered on this size range. From the 2.5 uL to 3.0 uL, it becomes more difficult to comtrol the droplet configuration and inconsistent data collection is more likely to occur.

The scheme used to introduce the droplets to the levitator is the product of months of refinement. For larger droplet sizes, the recommended procedure follows the steps outlined below.
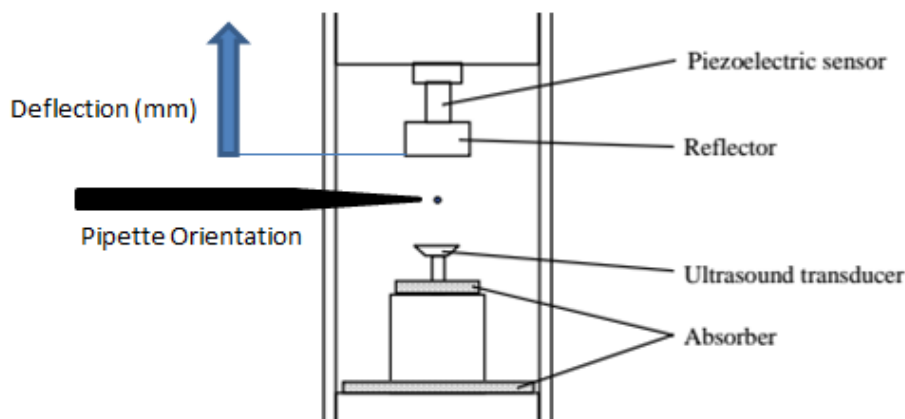
1) In order for the levitator to overcome the surface tension holding the droplet to the pipette, the micrometer adjustment screw should be lowered until the reflector is at the reference line, or zero deflection. This is the closest the reflector and transducer may come to one another.

2) The pipette should not be discharged until the pipette tip is ~1mm away from intersecting the standing wave. The pipette should then be depressed to the first stop, and brought close to the standing wave until the droplet is visibly affected by the standing wave power. The point at which the droplet is affected will be obvious, as its geometry will change from a sphere resting on the tip of the pipette to an oblate spheroid with one end of the major axis in the wave and one still held on the pipette tip.
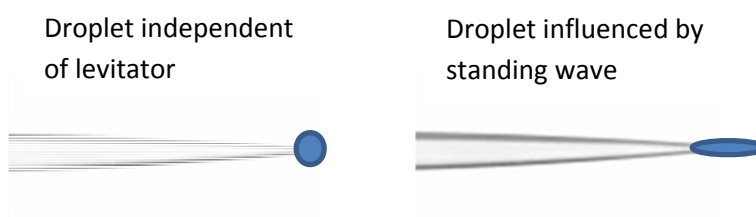

Figure 2B: Behavior of droplet in pipette

3) For droplets 2.0 uL or less, the pressure node will be sufficient to hold the droplet and overcome the surface tension between the droplet and pipette. As droplet size increases above ~2.5 uL, the pipette must be slowly dragged down and away from the node towards the transducer, which will provide enough additional force to remove the pipette without removing the droplet as well.

4) Once the pipette has been removed, the droplet will be severely flattened at the poles. To counter this, the micrometer adjustment screw can be used to increase the deflection and therefore the vertical distance between reflector and transducer. This decreases the force exerted on either pole of the droplet, and allows it assume a spherical shape.
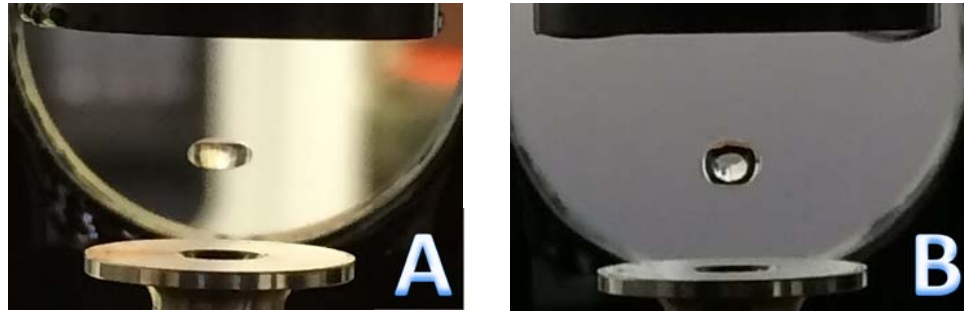
Figure 3B: Comparison of droplet shape for A) over-tightened setup and B) deflection to assume spherical shape

5) Once the droplet has assumed a stable configuration, the micrometer adjustment screw should be used to attain as spherical a shape as possible. If the distance between the transducer and reflector grows too large, the droplet will begin to wobble. It is best to increase the distance until the first horizontal movement occurs, and then readjust back down 50 microns.

It is important to note that while the levitation process is useful in isolating the droplet for irradiation, it also results in some fluid flow forced by the acoustic wave in which it is held. The average Reynolds number for a distilled water droplet held within the levitator is Re=1.83. Relative to fluid movement induced by irradiation, this flow profile is negligible.

APPENDIX C: BEAMGAGE SPECIFICATION

The most delicate adjustment is required for the BeamGage, which is mounted between the levitator and power meter. The chip on the BeamGage that registers power levels is unable to handle the full power of the laser, and thus shielding is required. The BeamGage utilizes neutral-density (ND) filters in order to reduce beam power and make the HEL safe for use with the gage. An ND filter serves to reduce the intensity of the radiation while preserving its distribution, so that the resulting profile matches the HEL in energy distribution, but with reduced intensity. This experiment used three such filters, each depending upon the power level that was being utilized.
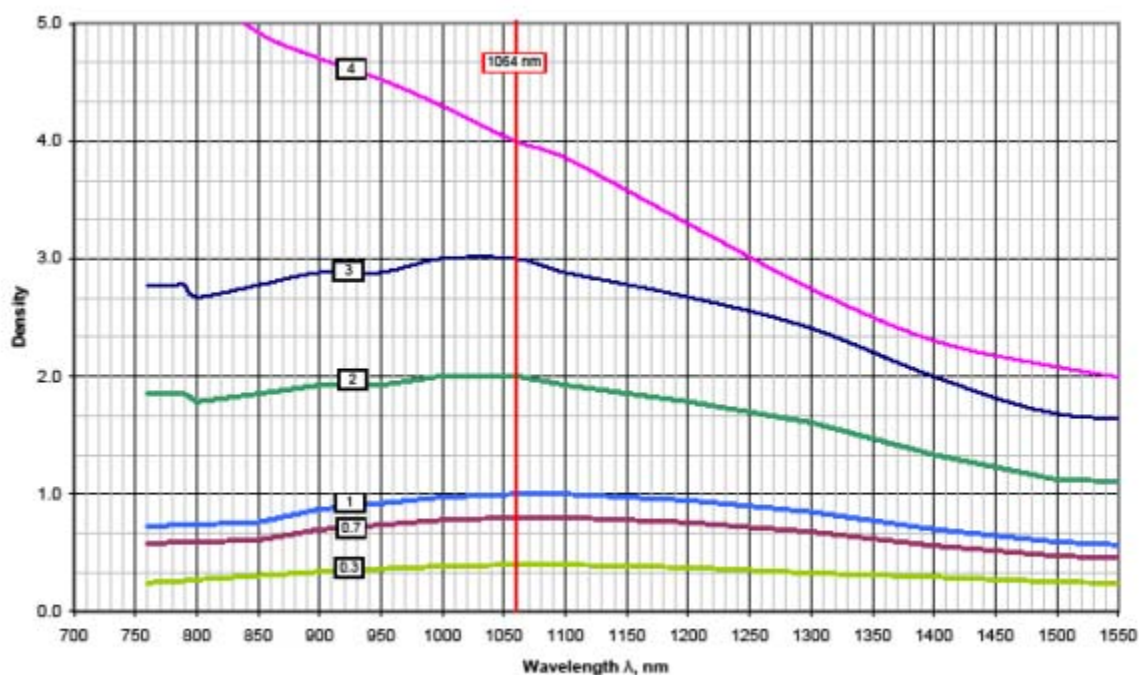
NIR filter set (Red Holders)

The ND filter slides into one of two filter ports, allowing for use of two filters at once to achieve a specific level of attenuation.
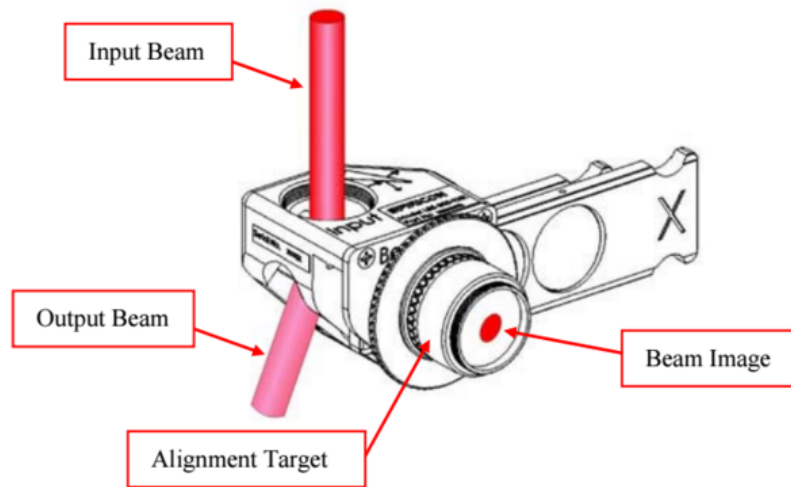

Figure 1C: BeamGage Schematic

Once the BeamGage has been properly calibrated for the appropriate power level of the HEL, the apparatus is aligned using micrometer adjustment in the same manner as the levitator. The beam image must be perfectly centered on the chip in order to collect a useable beam profile, which required a setup in which the adjustment does not traverse in the same direction as the levitator. The wedge used to split the beam screws onto the base of the BeamGage that collects the actual beam profile. When tightened completely, the face of the wedge is perpendicular to the beam, but the orientation of the beam image is not parallel with the face of the wedge
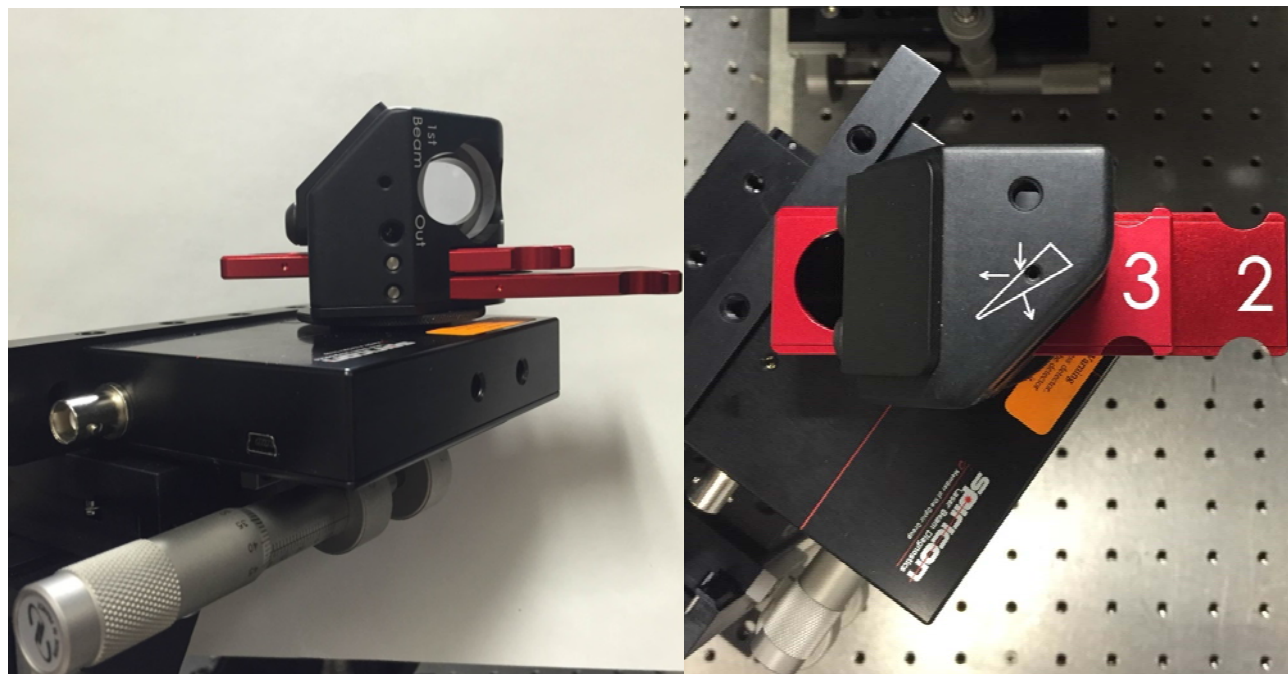
Figure 2C: Back view (left) and top view (right) of the BeamGage

As shown in Figure 2C, the fully tightened wedge does not have an edge line up in parallel with the gage in the rectangular lower portion. To compensate for this, one horizontal micrometer adjustment screw was attached to account for change in location horizontally. To ensure that the beam strikes the front face of the wedge perpendicularly, there is also a 360 degree swivel on the base of the BeamGage mount, allowing for all the necessary movement to align the profiler with the oncoming HEL beam.

Because the beam does not enter the profiler perpendicularly, the orientation of the profile is not the same as the droplet orientation. Figure 3C shows the relationship between droplet orientation and the resulting orientation of the beam profile. This is meaningful because observed trends within the beam profiles change with direction.
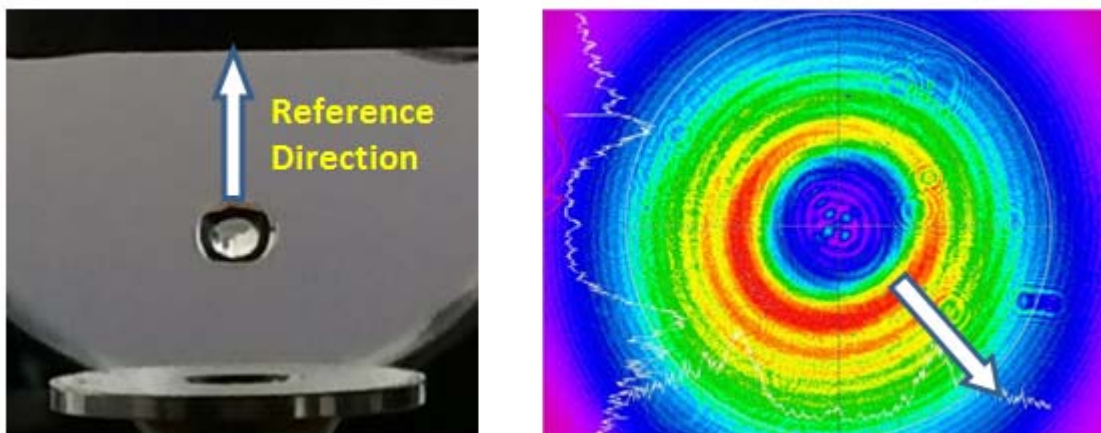
Figure 3C: Orientation of beam profile compared to droplet orientation

Between each run using the beam profiler, the guide beam was used in conjunction with a low magnitude ND filter to re-align the profiler with the new droplet size and shape. The difference in orientation made adjustment in all three directions necessary for the majority of runs.

APPENDIX D: IMAGE PROCESSING

The method for processing the images was developed utilizing a combination of built-in MatLab commands and personal code. The data collection process began with the capturing of video with the Hamamatsu camera, which was then temporarily saved to the hard drive to be processed. The code was compiled into function form, and resulted in a variety of items that could be included or excluded depending on the circumstances and goal of the particular run being processed. For example, all video frames and analysis sequencing could be saved selectively if a particular phenomenon had been discovered. The table below shows the basic form of the function and parameters returned.

Function Specifics:

Input	Output
	Drop Image and Analysis Progression
data_process (n,s,file_name)	Major Axis Length
	Minor Axis Length
n=total frames of video to analyze	Equivalent Diameter
s=sample rate (every "s" frames is analyzed)	Perimeter
file_name=save data, if desired	Area
	Eccentricity

Code:

```matlab
% Read and process images/videos
% Created for use with data acquired with imaqtool using the Hamamatsu camera
% Makes use of image processing toolbox


% ----------------------------------------------------------------------
% Open and view video. (Can also use Video Viewer app for quick viewing.)

clip = VideoReader('001.avi');
vidWidth = clip.Width;
vidHeight = clip.Height;

for n=1; %Initialize file writing
    n_final=1800; %Final frame you want to look at in the video
    frate=30; %frame rate
    s=30; %sample rate e.g. for s=50 every 50th frame is saved for anaylsis
    i=1;

    while n<n_final
        %folder='30NOV_vidprocess'; %Name of folder to write
        vid_frames=read(clip,n) ;
        %These can be added back in if you want to save the frames
        %imwrite(vid_frames, sprintf('%s/image_%d_frame_%d.png',folder,i,n)
);

        %J = imread(sprintf('%s/image_%d_frame_%d.png',folder,i,n));
        I=rgb2gray(vid_frames);
        subplot(2,4,7), imshow(I), title('Original Image');
```

```matlab
[~, threshold] = edge(I, 'sobel');
fudgeFactor = 1.0; %THIS IS CRUCIAL TO EFFECTIVE IMAGE MANAGEMENT
BWs = edge(I,'sobel', threshold * fudgeFactor);
subplot(2,4,1), imshow(BWs), title('Binary Gradient Mask');

% Dilate lines for better detection. Second argument in strel adjusts
% magnitude of dilation.
se90 = strel('line', 2, 90); %4 in for 2
se0 = strel('line', 2, 0);
BWsdil = imdilate(BWs, [se90 se0]);
subplot(2,4,2), imshow(BWsdil), title('Dilated Gradient Mask');

% Fill interior of object
BWdfill = imfill(BWsdil, 'holes');

subplot(2,4,3), imshow(BWdfill);
title('Binary Image with Filled Holes');

% Remove any misc objects on the border
BWnobord = imclearborder(BWdfill, 4);
subplot(2,4,4), imshow(BWnobord), title('Cleared Border Image');

% Smooth object
seD = strel('diamond',1);
BWfinal = imerode(BWnobord,seD);
BWfinal = imerode(BWfinal,seD);
subplot(2,4,5), imshow(BWfinal), title('Segmented Image');

% Create outline; show with original image
BWoutline = bwperim(BWfinal);
Segout = I;
Segout(BWoutline) = 255;
subplot(2,4,6), imshow(Segout), title('Outlined Original Image');

cc = bwconncomp(BWfinal, 4) ;
drop = false(size(BWfinal));
drop(cc.PixelIdxList{1}) = true;
imshow(drop);

%Save figure to same folder as the frame images
saveas(gcf,sprintf('%s/image_%d_props.png',folder,i))

conv=0.5; %convert pixels to mm
run=regionprops(cc,'all');

e_diam(i)=run.EquivDiameter;
area(i)=run.Area;
eccentricity(i)=run.Eccentricity;
maj_d(i)=run.MajorAxisLength;
min_d(i)=run.MinorAxisLength;
per(i)=run.Perimeter;

i=i+1;
```

```
        n=n+s; %How often to take sample- for frame rate=30, +30 samples
every second
    end
end
%%
% Currently set for 1800/30/30
t = table(e_diam',area',eccentricity',maj_d',min_d',per');
writetable(t,'Data_Distilled.xlsx');
```

The Analysis progression is a subplot that shows each step in the object detection progression which allows for measuring droplet dimensions. Each step performs a different function in
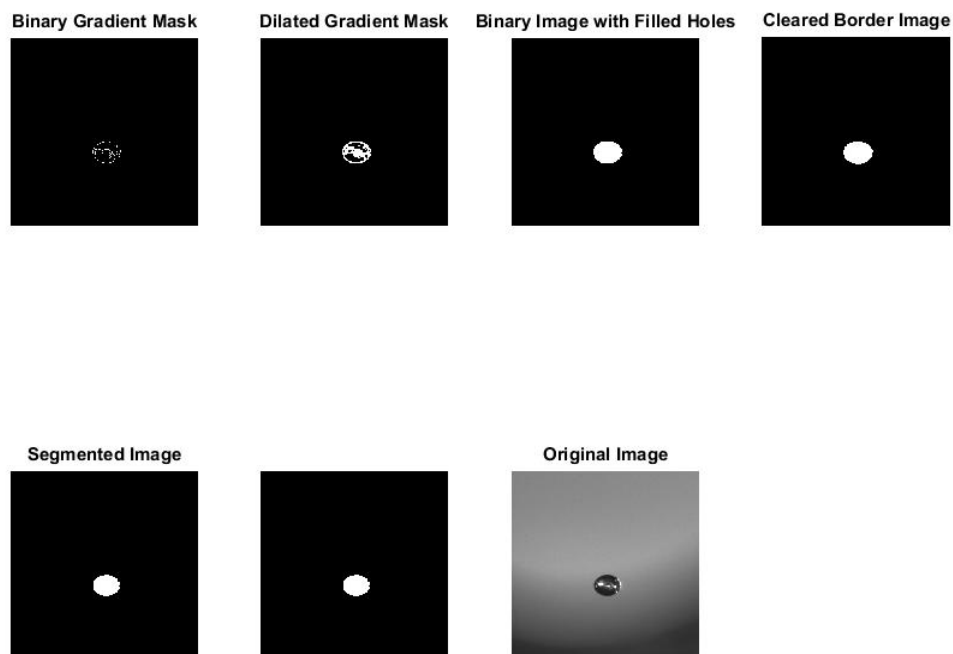
recognizing the droplet, utilizing the difference in gradient as the primary means to detect the droplet. The final image is then analyzed using a MatLab function, and the results are saved to an Excel file. The Excel file is then called for the plotting of the data.

Throughout the droplet detection and analysis, the image utilizes multiple scaling factors that allow for better detection depending upon the collection circumstances. These remain fairly consistent run to run, but when the droplet moves uncharacteristically it can cause a frame or two to go unrecognized, which results in outliers in the data set. A frequent cause is deficient dilation

for the gradient mask, resulting in a smaller area being filled than is appropriate. The dilation can be adjusted to mitigate these effects.

For the purposes of these experiments, the primary concern is with diameter and volume, a derived value based upon the diameter. The diameter is taken from the droplet parameters after the final image has been processed. Specifically, the diameter is an equivalent that accounts for the major and minor axis lengths. The diameter is not uniform around the entire droplet, as the standing wave creates pressure on both ends. Successful runs result in limited deformation, but the droplet shape tends to be an oblate spheroid more often than not. Therefore, MatLab calculates an equivalent diameter which is consequently used to find the change in volume with time over the irradiation of the droplet. This cross-sectional diameter is taken from $90°$ relative to the beam. Adjusting the camera position does not result in different diameters being registered, showing that the diameter is consistent when viewed from any viewing position in the same plane as the laser beam.

APPENDIX E: ABSORBANCE MEASUREMENT

Figure E1: Jasco V-670 NIR Spectrometer

A Jasco Spectrometer measurement was attempted to determine the absorption coefficient of both distilled and brackish water samples. Due to the low absorbance values encountered in the NIR spectrum, the values found were not in agreement with accepted values for distilled water. The photometric accuracy of the spectrometer used is +/- 0.02 absorbance units, and at the low values measured, the calculated absorptivity was within this range of error. Therefore, the absorption used for calculations was an accepted value found in a rigorous study of the photometric properties of distilled water [14].
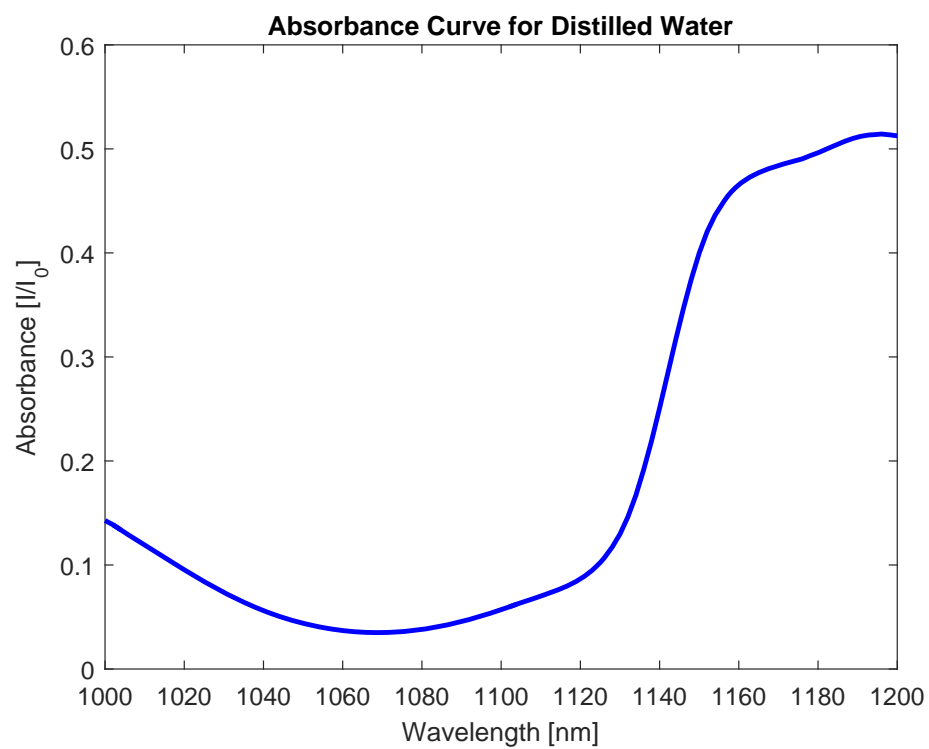
Figure E2: Absorbance Curve for Distilled Water